Biotechnology Journal

RESEARCH ARTICLE

Rational design and experimental evaluation of peptide ligands for the purification of adeno-associated viruses via affinity chromatography

Shriarjun Shastry[1,2] | Wenning Chu[1] | Eduardo Barbieri[1] | Paul Greback-Clarke[2] | William K. Smith[2] | Christopher Cummings[2] | Arianna Minzoni[1] | Jennifer Pancorbo[2] | Gary Gilleskie[2] | Kimberly Ritola[3,4] | Michael A. Daniele[4,5] | Thomas F. Johnson[6] | Stefano Menegatti[1,2,4,7]

[1]Department of Chemical and Biomolecular Engineering, North Carolina State University, Raleigh, North Carolina, USA

[2]Biomanufacturing Training and Education Center (BTEC), North Carolina State University, Raleigh, North Carolina, USA

[3]Neuroscience Center, Brain Initiative Neurotools Vector Core, University of North Carolina at Chapel Hill, Chapel Hill, North Carolina, USA

[4]North Carolina Viral Vector Initiative in Research and Learning (NC-VVIRAL), North Carolina State University, Raleigh, North Carolina, USA

[5]Joint Department of Biomedical Engineering, North Carolina State University and University of North Carolina at Chapel Hill, Raleigh, North Carolina, USA

[6]Department of Biochemical Engineering, University College London, London, UK

[7]LigaTrap Technologies LLC, Raleigh, North Carolina, USA

Correspondence
Gary Gilleskie, Biomanufacturing Training and Education Center (BTEC), North Carolina State University, 850 Oval Dr, Raleigh, NC 27606, USA.
Email: glgilles@ncsu.edu

Michael A. Daniele, North Carolina Viral Vector Initiative in Research and Learning (NC-VVIRAL), North Carolina State University, 911 Oval Dr, Raleigh, NC 27695, USA.
Email: mdaniel6@ncsu.edu

Stefano Menegatti, Department of Chemical and Biomolecular Engineering, North Carolina State University, 911 Partners Way, Raleigh, NC 27606, USA.
Email: smenega@ncsu.edu

Abstract

Adeno-associated viruses (AAVs) have acquired a central role in modern medicine as delivery agents for gene therapies targeting rare diseases. While new AAVs with improved tissue targeting, potency, and safety are being introduced, their biomanufacturing technology is lagging. In particular, the AAV purification pipeline hinges on protein ligands for the affinity-based capture step. While featuring excellent AAV binding capacity and selectivity, these ligands require strong acid (pH <3) elution conditions, which can compromise the product's activity and stability. Additionally, their high cost and limited lifetime has a significant impact on the price tag of AAV-based therapies. Seeking to introduce a more robust and affordable affinity technology, this study introduces a cohort of peptide ligands that (i) mimic the biorecognition activity of the AAV receptor (AAVR) and anti-AAV antibody A20, (ii) enable product elution under near-physiological conditions (pH 6.0), and (iii) grant extended reusability by withstanding multiple regenerations. A20-mimetic CYIHFS-GYTNYNPSLKSC and AAVR-mimetic CVIDGSQSTDDDKIC demonstrated excellent capture of serotypes belonging to distinct clones/clades – namely, AAV1, AAV2, AAV5, AAV6, AAV8, and AAV9. This corroborates the in silico models documenting their

---

Shriarjun Shastry and Wenning Chu are indicates equal contributions.

ability to target regions of the viral capsid that are conserved across all serotypes. CVIDGSQSTDDDKIC-Toyopearl resin features binding capacity ($\approx 10^{14}$ vp mL^{-1}) and product yields ($\approx$60%–80%) on par with commercial adsorbents, and purifies AAV2 from HEK293 and Sf9 cell lysates with high recovery (up to 78%), reduction of host cell proteins (up to 700-fold), and high transduction activity (up to 65%).

KEYWORDS

adeno-associated virus, affinity chromatography, gene therapy, peptide ligands, transduction activity

1 | INTRODUCTION

Viral vectors are poised to become fundamental tools in modern medicine and biotechnology owing to their role as delivery agents of gene therapies targeting rare diseases, oncolytic agents to fight aggressive forms of cancer, vaccine platforms to counter infectious diseases, and a gateway to engineer plants and animals for a sustainable agriculture.[1–4] The landscape of viral vector technology is rich of promises as much as challenges: novel vector designs are constantly being introduced with improved tissue targeting and gene delivery activity as well as lower genotoxicity, hepatotoxicity, and immunogenicity.[5–7] At the same time, the bioprocess technology utilized in viral vector manufacturing draws heavily upon a decades-old platform established decades ago for producing monoclonal antibodies (mAbs). This is well exemplified by the purification pipeline of adeno-associated viruses (AAVs, the vector of choice in gene therapy) where protein ligands that resemble the Protein A used for mAb purification are employed at the product capture step.[8,9]

The commercial landscape of affinity resins for AAV purification now counts six products, namely POROS™ CaptureSelect™ AAVX, AAV8 (CSAL8) and AAV9 (CSAL9), AVB Sepharose HP, Capto AVB, and AVIPure resins.[10,11] Owing to their high binding capacity and selectivity (needed to isolate AAVs from recombinant feedstocks, which typically feature low product titer and a wide abundance of impurities), these adsorbents have supported the clinical growth of gene therapy, providing a pathway to cure for patients with debilitating genetic diseases. At the same time, commercial affinity adsorbents suffer from high cost and impose the use of elution buffers (pH $\leq$3) that may affect the transduction activity of the viral vectors.[8,12]

Addressing the challenges inherent to current affinity technologies, our team has established a framework for developing peptide affinity ligands. Leveraging the chemical and structural diversity of peptides has delivered an ensemble of binders for protein purification that combine high selectivity and capacity with mild elution conditions: recent examples include ligands that release the product upon exposure to mild pH ($\geq$4),[13–16] kosmotropic salts (MgCl$_2$),[17] or light,[18,19] thus safeguarding the bioactivity of labile targets. The adoption of peptide ligands, which can be mass manufactured rapidly and affordably, is also conducive to reducing production costs. This is particularly *à propos* in the field of gene therapy, where manufacturing costs – to which the

purification segment contributes a great deal – result in price tags to patients ranging between \$2.5–3.5M.[20]

With the growing relevance of AAVs, amply documented by the surge in clinical trials and the uptick in regulatory approvals, we resolved to leverage our toolbox to develop AAV-targeting peptides. Relevant to our endeavor has been the wealth of data on AAV-targeting biomolecules, particularly the crystal structures of the complexes formed by AAVs of different serotypes with the AAV receptor (AAVR) and the anti-AAV antibody A20. Accordingly, we undertook the rational design of cyclic peptide mimetics of AAVR and A20 by abstracting sequences that target regions of the capsids that are highly conserved across serotypes of different clades. At the same time, to overcome the limitations of protein ligands, the peptide mimetics were designed to form complexes with different AAV serotypes that (i) feature high-affinity at physiological conditions ($|\Delta G_b| \geq 6.5$ kcal mol^{-1} at pH 7.4) and (ii) undergo a $\geq$100-fold loss of binding strength as the pH is lowered to 6.5. Among the selected sequences, A20-mimetic CYIHFSGYTNYNPSLKSC and AAVR-mimetic CVIDGSQSTDDDKIC demonstrated excellent capture of serotypes belonging to distinct clones/clades – AAV1, AAV2, AAV5, AAV6, AAV8, and AAV9 – corroborating the in silico models documenting their ability to target regions of the virion proteins that are conserved across all serotypes. CVIDGSQSTDDDKIC-Toyopearl resin features values of binding capacity ($\approx 10^{14}$ vp mL^{-1}) and product yields ($\approx$60%–80%) on par with commercial adsorbents, and purified AAV2 from a HEK293 cell lysate affording high recovery (70%–80%), a 700-fold reduction of host cell proteins (HCPs), and high transduction activity (up to 65%) of the purified viruses.

2 | MATERIALS AND METHODS

2.1 | In silico design of peptide mimetics of the AAV receptor (AAVR) and anti-AAV antibody A20

The crystal structures of AAVR in complex with AAV1 (PDB ID: 6JCQ and 7TI5), AAV2 (3J1S, 6IHB, and 6NZ0), AAV5 (7KP3 and 7KPN), and AAV9 (7WJX and 7WQP) as well as the complex of AAV2 with monoclonal antibody A20 (3J1S) were analyzed to identify the residues on the protein ligands (AAVR and A20) and

the AAV virion protein (VP1) involved in the affinity interaction and calculate their pairwise contributions to the binding energy. Based on this analysis, the A20-mimetic candidates CYGHFS-GYGNYGPC, CYGHFSPYGNYGPC, CYHFSYNYPC, CYHFSYNYPKSC, CYIHFSGYTNYNGSLKSC, CYIHFSGYTNYNPC, CYIHFSGYT-NYNPSLKSC, CYIHFSPYTNYNPSLKSC, CYVHFSGYSNYSPSC, GCGQQYWIGPFTFGCG, GQQYWIGPFTFG, LETVKPGLYEPITH-PRDYS, and SYDRPHTIPEYLGPKVTEL, and the AAVR-mimetic candidates AIVSPQFQEISLPTTSTVIDGSQSTDDDKIVQY, CDGSQST-DDDKIC, CDSQSTDDDKIC, CSGSTDDDKIC, CSGSTEQEKIC, CVIDGSQSTDDDKIC, CVIDGSQSTDDDKIVQYC, GCLITHPRDYS, GCLITHPRDYSGCG, GYIHFSGYTNYNPSLKS, GYWIGPFTGGGYI-HFSGYT, GYWIGPFTGPGYIHFSGYT, GYWIGPFTPGPYIHFSGYT, LITHPRDYSPKLTPGLYEFG, and TVIDGSQSTDDDKIVQY were constructed using the molecular editor Avogadro[21] and their structures were prepared in GROMACS using the force field GROMOS 54A7.[22] The disulfide-cyclic peptide sequences A1-A12 were designed in the cyclic format GC-$X_1X_2[...]X_n$-C-GSG, whereas linear peptide sequences A12–A16 were designed in the linear format G-$X_1X_2[...]X_n$-GSG. Each peptide sequence was (i) placed in a simulation box with periodic boundary containing 1500 TIP3P water molecules and equilibrated with 10,000 steps of steepest gradient descent; (ii) heated to 300 K in an NVT ensemble for 250 ps using 1 fs time steps; and (iii) equilibrated to 1 atm via a 500-ps NPT simulation with 2 fs time steps. The production runs were conducted in the NPT ensemble under constant 300 K and 1 atm by applying the Nosé-Hoover thermostat and the Parrinello-Rahman barostat, respectively.[23] The motion equations were integrated using the leap-frog algorithm with steps of 2 fs. The covalent bonds were constrained using the LINCS algorithm. The Lennard-Jones and short-range electrostatic interactions were calculated using cut-off values of 0.8 and 1.2 nm, respectively. The particle-mesh Ewald method was implemented for the long-range electrostatic interactions.[24–26] The lists of bonded and non-bonded interactions (cutoff of 1.2 nm) were updated every 2 and 6 fs, respectively. The energetic landscape associated to the various peptide conformations was sampled to identify the structures with absolute energy minima. The structure of the VP1 from AAV1 (PDB ID: 6JCR), AAV2 (6IH9), AAV3 (3KIC), AAV4 (2G8G), AAV5 (7KP3), AAV6 (5EGC), AAV7 (7JOT), AAV8 (2QA0), and AAV9 (7WJX) were initially prepared using Protein Prep Wizard (PPW, Schrödinger, New York, NY)[27] by correcting missing residues or atoms, adding explicit hydrogens, removing salt ions, and optimizing the hydrogen-bonding network. The resulting VPs were utilized to construct triangular clusters of VP1-VP2-VP3 proteins, whose ionization states at pH 6.0 and 7.4 were obtained – and the corresponding structural minimization of the clusters were performed using PROPKA.[28] The construct triangular clusters were finally draped on the spherical cap of the corresponding AAV capsid. The peptide ligands were then docked in silico against the AAVR binding sites using the docking software HADDOCK (High Ambiguity Driven Protein-Protein Docking) v.2.4.[29,30] The AAVR-binding residues and the A20-binding residues on the VP proteins and residues $X_1X_2[...]X_n$ on the peptides were denoted as "active," while all surrounding residues were marked as "passive." Clusters of

up to 20 docked AAV:peptide structures selected based on Cα RMSD <7.5 Å were ranked using the dMM-PBSA score.[31] Finally, the top AAV:peptide complexes were refined via 200-ns MD simulations to estimate the free energy of binding (ΔG_B).

2.2 | Materials

Fluorenylmethoxycarbonyl- (Fmoc-) protected amino acids Fmoc-Ala-OH, Fmoc-Arg(Pbf)-OH, Fmoc-Asn(Trt)-OH, Fmoc-Asp(OtBu)-OH, Fmoc-Cys(Trt)-OH, Fmoc-Glu(OtBu)-OH, Fmoc-Gly-OH, Fmoc-His(Trt)-OH, Fmoc-Ile-OH, Fmoc-Leu-OH, Fmoc-Lys(Boc)-OH, Fmoc-Phe-OH, Fmoc-Pro-OH, Fmoc-Ser(tBu)-OH, Fmoc-Thr(tBu)-OH, Fmoc-Trp(Boc)-OH, Fmoc-Tyr(tBu)-OH, and Fmoc-Val-OH, the coupling agent Hexafluorophosphate Azabenzotriazole Tetramethyl Uronium (HATU), diisopropylethylamine (DIPEA), piperidine, and trifluoroacetic acid (TFA) were procured from ChemImpex International (Wood Dale, IL). The Toyopearl NH2-750F resin (pore size >100 nm; particle size: 45 μm; ligand density: 200 μmol mL^{-1} resin) was obtained from Tosoh Bioscience (Tokyo, Japan). Triisopropylsilane (TIPS), Kaiser test kits, 1,2-ethanedithiol (EDT), polybrene, and phosphate buffered saline (PBS) tablets were from MilliporeSigma (St. Louis, MO, USA). Dichloromethane (DCM), methanol, N-methyl-2-pyrrolidone (NMP), N,N'-dimethylformamide (DMF), Bis-Tris HCl, magnesium chloride (MgCl$_2$), phosphoric acid, potassium chloride (KCl), sodium chloride (NaCl), sodium hydroxide (NaOH), Pluronic™ F-68, POROS™ CaptureSelect™ AAVX Affinity Resin, and SilverQuest™ Silver Staining Kit were obtained from Fisher Chemical (Hampton, NH, USA). The AVB Sepharose HP was sourced from Cytiva (Marlborough, MA). Dulbecco's Modified Eagle Medium (DMEM) and fetal bovine serum (FBS), Gibco™ Viral Production Cells 2.0, AAV-MAX Enhancer, Viral-Plex™ Complexation Buffer, Transfection Reagent, benzonase endonuclease, and AAV-MAX Lysis Buffer were obtained from ThermoFisher Scientific (Waltham, MA). Human fibrosarcoma (HT1080) cells were sourced from ATCC (Manassas, VA). Pure AAV2, AAV6, AAV8, and AAV9 were sourced from Charles River Laboratories (Durham, NC). The Alltech chromatography columns (diameter: 3.6 mm; length: 50 mm; volume: 0.5 mL), and 10 μm polyethylene frits were obtained from VWR International (Radnor, PA, USA). The AAV ELISA kits were purchased from Progen (Wayne, PA) while the HEK293 ELISA kits were purchased from Cygnus (Southport, NC). The BioResolve SEC mAb Column (particle diameter: 2.5 μm; pore diameter: 200 Å; column diameter: 7.8 mm; column length: 300 mm) size exclusion chromatography column was from Waters Inc. (Milford, MA). The CIMac PrimaS™ 0.1 mL analytical monolith column (diameter: 5.2 mm; length: 4.95 mm; volume: 0.1 mL, channel radius: 1050 nm) for steric exclusion chromatography analysis was obtained from BIA separations (Ajdovscina, Slovenia). The 10%–20% Tris-Glycine HCl SDS-PAGE gels were purchased from Bio Rad Life Sciences (Hercules, CA). In-house production of AAV6, AAV8, and AAV9 were conducted using plasmids from Aldevron. Plasmids pAAV2/9n, pAAV2/8, and pAdDeltaF6 were a gift from James M. Wilson (Addgene plasmid #112865, #112864, and #112867, respectively). Plasmid pDGM6 was a gift from David Russell

(Addgene plasmid #110660).[32] Plasmid pAAV CAGG eGFP was a gift from Troy Margrie (Addgene plasmid #107707).[33]

2.3 | Synthesis of peptide ligands on Toyopearl resin.

Sequences CYIHFSGYTNYNPSLKSC (A1), CYIHFSGYTNYNGSLKSC (A2), CYVHFSGYSNYSPSC (A3), CYGHFSGYGNYGPC (A4), CYGHF-SPYGNYGPC (A5), CYIHFSGYTNYNPC (A6), CYIHFSPYTNYNPC (A7), CYHFSYNYPKSC (A8), CYHFSYNYPC (A9), CVIDGSQSTDDDKIC (A10), CDGSQSTDDDKIC (A11), CDSQSTDDDKIC (A12), CSGSTD-DDKIC (A13), GYWIGPFTGGGYIHFSGYT (A14), GYWIGPFTGPGYI-HFSGYT (A15), GYWIGPFTPGPYIHFSGYT (A16), and LITHPRDYS-PKLTPGLYEFG (A17) were synthesized on Toyopearl NH2-750F (TP750F) resin using an Initiator+ Alstra™ automated peptide synthesizer (Biotage, Uppsala, Sweden). Each amino acid coupling step was performed using 3 equivalents (eq.) of Fmoc/tBu-protected amino acid, 3 eq. of HATU and 0.5 M, 6 eq. of DIPEA – all at the concentration of 0.5 M – in dry DMF at 45°C for 20 min. The yield of all amino acid coupling steps was monitored via Kaiser test, while the removal of Fmoc groups was performed using 20% v/v piperidine in DMF at room temperature for 30 min. The final peptide density varied within the range of 0.11–0.16 mmol g^{-1} of resin. Following chain elongation, the peptides were deprotected via acidolysis using a cleavage cocktail containing TFA, thioanisole, anisole, and EDT (94/3/2/1) for 2 h. After deprotection, the peptide-TP750F resins were washed sequentially with DCM, DMF, methanol, and stored in 20% v/v aqueous methanol.

2.4 | Production and harvest of AAV2 from HEK293 cell cultures

Gibco™ Viral Production Cells 2.0 were initially diluted to 3.0×10^6 cells mL^{-1} incubated with AAV-MAX Enhancer at 1% v/v in a humidified incubator with 8% CO_2 while shaken at 120 rpm at 37°C. The transfection cocktail was prepared by combining the pRC2 plasmid, which contains the REP and CAP genes for AAV2, the pHelper plasmid, which contains helper genes necessary for AAV replication, and the pAAV-GFP plasmid, which containing the GFP gene to be packaged into the newly formed AAVs, at the molar DNA ratio of 1:1:1 (pRC2: pHelper: pAAV-GFP) and the total concentration of 1.5 μg mL^{-1} of culture. The plasmid cocktail was diluted in Viral-Plex™ Complexation Buffer to 10% of the culture volume. In parallel, volumes of Transfection Booster and Transfection Reagent corresponding to 0.3% and 0.6% of the culture volume were mixed. The DNA/Viral-Plex and the Transfection Booster/Transfection Reagent components were incubated at room temperature for 10 min, mixed, and incubated with the Gibco™ Viral Production Cells at room temperature for 20 min, after which the cells were returned to the humidified incubator. After 72 h, AAV-MAX Lysis Buffer was added at a volume corresponding to 10% of the culture volume to lyse cells. The cell lysate was subsequently added with 2 mM $MgCl_2$ and 90 U mL^{-1} benzonase endonuclease (GENIUS™

Nuclease) and incubated at 37°C for 2 h. The lysate was then clarified via centrifugation at $4100 \times g$ for 40 min and the resulting supernatant was collected.

2.5 | Preparation of feed samples

Clarified HEK293 cell lysates containing AAV1 and AAV5 were obtained from UNC Vector core (Chapel Hill, NC). Clarified HEK293 cell lysates containing AAV2, AAV6, AAV8, and AAV9 were prepared in duplicate as described in Section 2.4, while the clarified Sf9 cell lysate containing AAV2 was obtained from BTEC (Raleigh, NC). The AAVs were isolated from the lysates via iodixanol density gradient centrifugation and their titer was adjusted to ≈5.0×10^{11}–5.0×10^{12} vp mL^{-1} via tangential flow filtration against 20 mM NaCl in 10 mM Bis-Tris at pH 7.0 using filters with MWCO of 300 kDa. Finally, the HEK293 and Sf9 cell culture lysates containing AAV2 were diafiltered against 20 mM NaCl in 10 mM Bis-Tris at pH 7.0 to achieve a final AAV2 titer of ≈1.9×10^{12} vp mL^{-1}, and a HCP titer of ≈0.3 mg mL^{-1} in the HEK293 harvests and ≈1.1 mg mL^{-1} in the Sf9 harvest.

2.6 | Binding studies of AAV1, AAV2, AAV5, AAV6, AAV8, and AAV9 in non-competitive conditions using peptide-TP750F resins

A volume of 0.5 mL of POROS™ CaptureSelect™ AAVX affinity resin, AVB Sepharose HP resin, (A1) CYIHFSGYTNYNPSLKSC-, (A2) CYIHFSGYTNYNGSLKSC-, (A3) CYVHFSGYSNYSPSC-, (A4) CYGHFSGYGNYGPC-, (A5) CYGHFSPYGNYGPC-, (A6) CYIHFSGYTNYNPC-, (A7) CYIHFSPYTNYNPC-, (A8) CYHFSYNYPKSC-, (A9) CYHFSYNYPC-, (A10) CVIDGSQSTDDDKIC-, (A11) CDGSQSTDDDKIC-, (A12) CDSQSTDDDKIC-, (A13) CSGSTDDDKIC-, (A14) GYWIGPFTGGGYIHFSGYT-, (A15) GYWIGPFTGPGYIHFSGYT-, (A16) GYWIGPFTPGPYIHFSGYT-, and (A17) LITHPRDYSPKLTPGLYEFG-TP750F resins was initially packed in an Alltech chromatography column and washed with 10 column volumes (CVs) of 20% v/v ethanol, 10 CVs of MilliQ water, and 10 CVs of binding buffer (10 mM Bis-Tris, 20mM NaCl buffer at pH 7.0). A volume of 10 mL of pure AAV solution in binding buffer was loaded on the column at the flow rate of 0.17 mL min^{-1} (residence time, RT: 3 min). The resin was washed with 20 CVs of binding buffer at 0.5 mL min^{-1}. The bound AAVs were eluted from the peptide-TP750F resins using 1 M $MgCl_2$ in 10 mM Bis-Tris HCl buffer at pH 6.0 at the flow rate of 0.5 mL min^{-1} (RT: 1 min). Elution from POROS™ CaptureSelect™ AAVX affinity resin and AVB Sepharose HP resin was conducted using 0.2 M $MgCl_2$ in 200 mM citrate buffer at pH 2.2 and PBS at pH 2.0 at the flow rate of 0.25 mL min^{-1} (RT: 2 min). All resins were regenerated with 10 CVs of phosphate buffered saline at pH 2.0 at the flow rate of 0.5 mL min^{-1}. All dynamic binding experiments were performed using a ÄKTA Avant system from Cytiva (Marlborough, MA), while continuously monitoring the effluent stream via UV spectrometry at 280 nm. The collected

fractions were analyzed using serotype-specific AAV ELISA Kit as described in Section 2.9 to quantify the values of AAV binding and recovery.

2.7 | Dynamic AAV2 binding capacity of peptide-TP750F resins

A volume of 0.5 mL of POROS™ CaptureSelect™ AAVX affinity resin, AVB Sepharose HP resin, (A1) CYIHFSGYTNYNPSLKSC-TP750F resin, (A4) CYGHFSGYGNYGPC-, and (A10) CVIDGSQSTDDDKIC-TP750F resins were initially packed and equilibrated with binding buffer as described in Section 2.6. A volume of 45 mL of HEK293 cells lysate containing AAV2 and diafiltered into binding buffer was loaded on the column at the flow rate of 0.17 mL min^{-1} (residence time, RT: 3 min). Resin washing and elution of bound AAV2 from the peptide-TP750F resins and the commercial resins was performed as described in Section 2.6. All dynamic binding experiments were performed using a ÄKTA Avant system from Cytiva (Marlborough, MA), while continuously monitoring the effluent stream via UV spectrometry at 280 nm. The collected fractions were analyzed by AAV2 ELISA Kit as described in Section 2.9 to generate the breakthrough curves, and the resulting chromatograms were utilized to calculate the DBC$_{10\%}$.

2.8 | Purification of AAV2 and AAV6 from clarified HEK293 and Sf9 cell lysate using peptide-TP750F resins

A volume of 0.5 mL of POROS™ CaptureSelect™ AAVX affinity resin, AVB Sepharose HP resin, (A1) CYIHFSGYTNYNPSLKSC-, (A3) CYVHFSGYSNYSPSC-, (A4) CYGHFSGYGNYGPC-, (A6) CYIHFSGYTNYNPC-, (A10) CVIDGSQSTDDDKIC-, and (A12) CDSQSTDDDKIC-TP750F resins were initially packed and equilibrated with binding buffer as described in Section 2.6. A volume of 10 mL of clarified HEK293 cell culture lysate containing either AAV2 at ≈1.9 × 10^{12} vp mL^{-1} (HCPs titer ≈0.30 mg mL^{-1}) or AAV6 at ≈2.1 × 10^{12} vp mL^{-1} (HCP titer ≈0.28 mg mL^{-1}) was loaded at the flow rate of 0.17 mL min^{-1} (RT: 3 min). Resin washing and elution of bound AAV2 from the peptide-TP750F resins and the commercial resins was performed as described in Section 2.6. All resins were regenerated with 10 CVs of PBS buffer at pH 2.0 at the flow rate of 0.5 mL min^{-1} and re-used for 20 additional cycles of AAV2 purification. The collected flow-through and elution fractions were analyzed by ELISA Kit (see Section 2.9) to determine the values of AAV2 and AAV6 yield, HEK293 and Sf9 ELISA Kit (see Section 2.10) to quantify the values of HCP removal, size exclusion chromatography (see Section 2.11) and steric exclusion chromatography (see Section 2.12) to measure global product purity, transmission electron microscopy (see Section 2.13) to evaluate the integrity of eluted AAVs, and fluorescence flow cytometry (see Section 2.14) to quantify the transduction efficiency of the eluted AAVs.

2.9 | Capsid quantification via serotype-specific AAV ELISA kits

The AAV titer in the feed, flow-through, and elution samples collected as described in Sections 2.6–2.8 was measured using AAV Titration ELISA kit (PROGEN, Wayne, PA) following the manufacturer's protocol.

2.10 | Quantification of HCPs

The titer of HEK293 and Sf9 HCPs in the feed, flow-through and elution samples collected as described in Section 2.8 was measured using a Generation 3 HEK293 HCP ELISA kit and a Generation 2 Sf9 HCP ELISA kit (Cygnus Technologies, Southport, NC) following the manufacturer's protocols.

2.11 | Analytical size-exclusion chromatography (SEC)

The feed, flow-through, and elution samples collected as described in Section 2.8 were analyzed by SEC HPLC using a BioResolve SEC column (Waters, Milford, MA) operated with a 40-min isocratic method using PBS at pH 7.0 (0.05% v/v sodium azide) at the flow rate of 0.50 mL min^{-1}. A volume of 10 μL of sample was injected and the effluent continuously monitored via UV (abs: 260 nm and 280 nm) fluorescence spectroscopy (ex/em: 280/350 nm).

2.12 | Analytical steric-exclusion chromatography (SXC)

The feed, flow-through, and elution samples collected as described in Section 2.8 were analyzed via analytical SXC using a monolith 0.1 mL CIMac PrimaS™ analytical column (BIA Separations, Slovenia) operated with a 20-min linear gradient from 100:0 A:B to 0:100 A:B (mobile phase A: 10% v/v PEG 6K in PBS at pH 7.0; mobile phase B: 3X PBS at pH 7.0) at the flow rate of 0.33 mL min^{-1}. Injection volumes were normalized based on the AAV titer measured via ELISA kits as described in Section 2.9. The effluent continuously monitored via fluorescence spectroscopy (ex/em: 280/350 nm).

2.13 | AAV imaging via transmission electron microscopy (TEM)

The sample grids were glow discharged using the Pelco easiGlow™ unit and taken to a biosafety cabinet, where 3 μL of sample was added on the grid and incubated for 60 s at room temperature. Each sample was then blotted using a Whatman paper, and 5 μL of MilliQ water was added on the grid and blotted for 3 times. Finally, 3 μL of 1% v/v Nano-W stain was added on the grid, incubated for 5 s, and

blotted. The sample grid was dried in a desiccator for 15 min and placed in a clean sponge box overnight. The sample grids were imaged using a miniTEM™ system (Vironova, Stockholm, Sweden) using the VIAS software for image collection and analysis.

2.14 | Fluorescence flow cytometry (FFC)

HT1080 cells were cultured in DMEM media supplemented with 10% v/v FBS at 5% CO_2 and 37°C until reaching 80%–90% confluence. Cells were then seeded in 96-well plates at a density of 10,000 cells per well and cultured overnight. The AAV in the HEK293 cell lysate and the eluted samples were serially diluted in DMEM (no FBS and antibiotics) added with polybrene at 8 μg mL^{-1}. An initial study was conducted to optmize the Multiplicity of infection (MOI) coefficient by incubating either 10^7, 10^8, 10^9, or 10^{10} viral genome copies with 10^4 HT1080 cells (MOIs: 10^3, 10^4, 10^5, and 10^6). We concluded – in line with what found in the literature – that the MOI of 10^4 is optimal for our transduction assay on HT1080. Accordingly, to quantify the transduction activity of the AAVs purified in this study, a volume of 0.1 mL of either cell lysate or elution fraction was incubated with the HT1080 cells at the MOI of 10^4. After 24 h, spent medium was replaced with fresh DMEM supplemented with 10% v/v FBS and the cells were cultured for 72 h. The fraction of cells expressing GFP (GFP$^+$) was quantified using a CytoFlex flow cytometer (Beckman Coulter, Brea, CA) and the number of transduction units per mL (TU mL^{-1}) was calculated using Equation (1):

$$\text{Activity}\left(\frac{\text{TU}}{\text{mL}}\right) = \frac{N_{\text{HT1080}} \times \%\text{GFP}^+}{V \times DF} \tag{1}$$

wherein N_{HT1080} is the number of cells incubated with the diluted AAV sample, V is the volume of the diluted AAV sample, and DF is the dilution factor. Finally, the values of relative transduction efficiency (RTE) were calculated using Equation (2), namely as the ratio of transduction efficiency (TE) of eluted AAVs versus fed AAVs.

$$\text{RTE}\,(\%) = \frac{\text{TE}\rfloor_{\text{Elution}}}{\text{TE}\rfloor_{\text{Feed}}} = \frac{\frac{\text{Transducing units}}{\text{Viral particles}}\bigg\rfloor_{\text{Elution}}}{\frac{\text{Transducing units}}{\text{Viral particles}}\bigg\rfloor_{\text{Feed}}} \times 100 \tag{2}$$

3 | RESULTS AND DISCUSSION

3.1 | Rational design of AAVR-mimetic and A20-mimetic peptides

A number of biological ligands targeting AAV are known to date, including transmembrane receptor proteins and engineered proteins. Tissue targeting and cell access by AAVs is mediated by (i) attachment factors, also known as "primary receptors," namely glycan moieties (e.g., sucrose octasulfate, sialic acid, and galactose) that feature promiscuous low-affinity capsid binding and whose role is to accumulate AAV at the cell surface; and (ii) cell surface receptors that specifically interact

with AAV and whose binding is required to initiate viral cell entry. To date, known receptors and their target serotypes include oligosaccharides heparin (AAV2) and fondaparinux (AAV-DJ) as well as the AAV receptor (AAVR), a 150 kDa glycoprotein required for cell transduction by several serotypes (AAV1, AAV2, AAV3B, AAV5, AAV6, AAV8, and AAV9). AAVR comprises multiple domains, known as Ig-like polycystic kidney disease repeat domains (PKD)[34,35]: for example, AAV2 is bound by PDK1-3, AAV5 predominantly interacts with PKD1, while AAV1 and AAV8 require a combination of PKD1 and PKD2. Additionally, AAV2 targets integrins, fibroblast growth factor receptor (FGFR1), $\alpha V\beta 5$, and $\alpha 5\beta 1$.[36–38] AAV2, AAV3, AAV8, and AAV9 capsid proteins have been found to bind the laminin receptor displayed on the surface of yeast cells.[39] AAV2 and AAV3 bind FGFR1,[37,40] the hepatocyte growth factor receptor (HGFR),[41] while AAV5 and AAV6 respectively target the platelet-derived growth factor receptor (PDGFR) and the epidermal growth factor receptor (EGFR).[42] Besides natural receptors, a number of anti-AAV monoclonal neutralizing antibodies have been developed, including mNAbs ADK1a, 4E4, and ADK6 targeting AAV1, mNAbs A20 and C37-B targeting AAV2, mNAbs ADK5b and HL2476 and mAbs ADK5a and 3C5 targeting AAV5, and mNAbs ADK5a and ADK6 targeting AAV6, and mAb ADK8 targeting AAV8. Finally, single-chain camelid antibody fragments and small protein scaffolds have been developed as affinity ligands for purifying AAVs from recombinant cell lysates. These include the: serotype-agnostic AAVX and the AAV8- and AAV9-targeting CSAL8 and CSAL9 introduced by ThermoFisher, the serotype-agnostic AVB by Cytiva, and AVIPure® AAV2, AAV8, and AAV9 developed by Repligen for the corresponding serotypes.

Despite the abundance of AAV-binding ligands, only the crystal structures of AAVR in complex with AAV1 (PDB ID: 6JCQ and 7TI5), AAV2 (6IHB and 6NZ0), AAV5 (6JCS), and AAV9 (7WJX) as well as the complex of AAV2 with monoclonal antibody A20 (3J1S) are reported. The analysis of pairwise interactions between the active residues on AAVR and A20 and the targeted residues on the virion protein (VP1, Figure S1 and Table S1) identified critical AAV-binding residues and motifs. These were utilized to design an in silico ensemble of candidate ligands, whose sequence, structure, and key physicochemical parameters are reported in Table S2. As can be gathered from the sequence homology and the values of root-mean-square deviation (RMSD) of the atomic positions of the peptides *vs.* their cognate proteins, the proposed library spans a wide space of chemical and structural diversity as well as similarity with A20 and AAVR.

The peptides were docked in silico against the homology spherical cap structures of AAV1, AAV2, AAV5, AAV6, AAV8, and AAV9. These were created by collating the published structures of VP1 into the triangular asymmetric units that form the icosahedral AAV capsid.[9] Prior to docking, the triangular clusters were equilibrated to two values of pH – 7.4, which is utilized during adsorption, and 6.0, which is adopted for the product release. An initial round of "blind" docking was performed to evaluate the ability of the designed sequences to target the known binding sites of A20 and AAVR. In order to mimic the orientational constraint imposed upon the peptides by their conjugation onto the surface of the chromatographic resin, the -GSG tripeptide
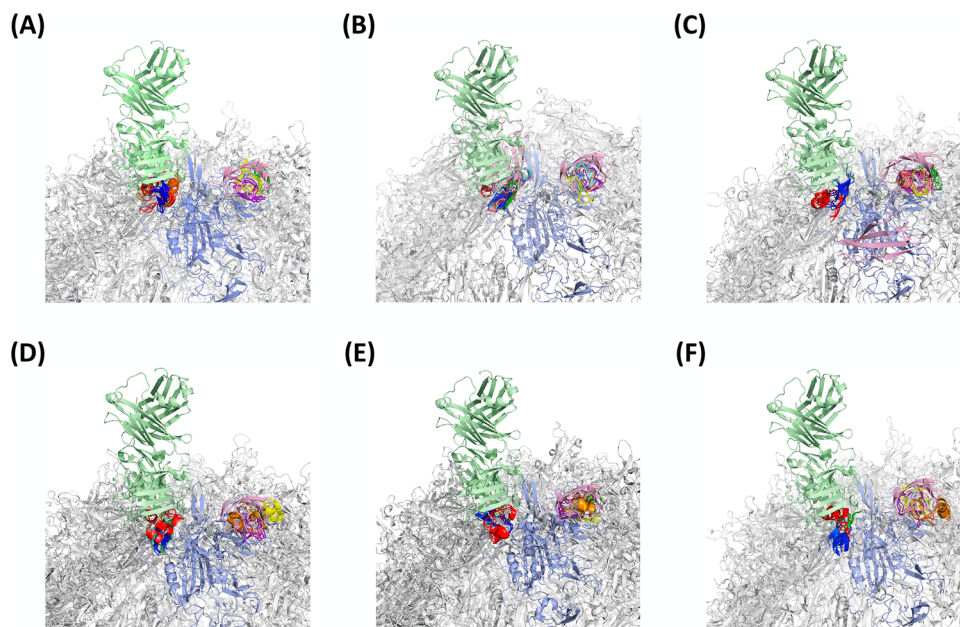
FIGURE 1 Representative complexes formed by A20-mimetic peptides CYIHFSGYTNYNPSLKSC (A1, red), CYGHFSGYGNYGPC (A4, green), CYIHFSGYTNYNPC (A6, blue), CVIDGSQSTDDDKIC (A10, yellow), CDGSQSTDDDKIC (A11, magenta), and LITHPRDYSPKLTPGLYEFG (A17, orange) with the capsids of (A) AAV1 (PDB IDs: 6JCQ, 6JCR, 7RK9, and 8FQ4), (B) AAV2 (5IPI, 6IH9, 6IHB, and 6U0V); (C) AAV5 (6JCS, 6JCT, 7KP3, and 7KPN); (D) AAV6 (3SHM, 3OAH, 4V86, and 5EGC); (E) AAV8 (2QA0, 3RAA, 6PWA, 6U2V, and 6V10); and (F) AAV9 (3UX1, 7MT0, 7WJW, and 7WJX) obtained via molecular docking and dynamics simulations at pH 7.4 and ionic strength of 150 mM. The AAVR and the A20 antibody are presented as light pink and light green cartoons, respectively. The VP1 is presented as light blue cartoon, while the remainder of the capsid is presented in light gray cartoon.

appended on the C-terminal end of the peptides was constrained not to bind AAV.[13,17,19,43–49] Selected AAV:peptide complexes (those comprising more than 20 peptide clusters) were refined via 250-ns MD simulations in explicit solvent at both pH 7.4 and 6.0 to obtain reliable values of binding free energy (ΔG_b). Representative complexes formed by the selected peptides on the target serotypes are shown in Figure 1, while the values of binding energy and the corresponding dissociation constant ($K_{D,in silico}$) are listed in Tables 1 and 2. Finally, detailed results of A1, A4, and A10 docking on the target AAV1, AAV2, AAV5, AAV6, AAV8, and AAV9 are reported in Figures S2.

Our in silico results show that 17 of the 28 sequences originally designed and listed in Section 2.1 bind all target serotypes, forming binding poses that overlap with those of the AAVR:AAV and A20:AAV2 complexes (Figure 1). Most notably, nine A20-mimetic peptides formed true affinity interactions ($|\Delta G_b| > 6.5$ kcal mol^{-1} at pH 7.4) with all serotypes, despite the cognate A20 being designed as an anti-AAV2 antibody. This can be attributed to the cyclic format of these candidate ligands, whose rigidity decreases the entropic penalty to the binding energy that is characteristic of their linear, and hence more flexible, counterparts. As anticipated, however, shorter sequences (A5–A9) exhibited lower binding energies (binding energy $|\Delta G_b| < 7.5$ kcal mol^{-1}) than longer variants (A1–A4) whose higher number of amino acids provides a stronger enthalpic contribution to the binding energy. Particularly notable was the case of CYIHFS-GYTNYNPSLKSC (A1) whose dominant binding site on AAV1, AAV2, AAV5, AAV6, and AAV8 ($|\Delta G_b| \approx 7.7–9$ kcal mol^{-1} at pH 7.4) shares

>90% of paired interactions with A20. We also noted that the shortest A20-mimetics (A6–A9) appeared to form multiple low-affinity binding poses on the various serotypes, which do not overlap with the binding sites of either A20 or AAVR. This can be imputed to their smaller hydrodynamic radius (Table S2), which enables these peptides to fit druggable sites displayed on the capsid surface that are precluded to larger binders. As observed in a prior study,[9] the solvent-accessible convex surface of AAV capsids present multiple sites that are highly conserved across serotypes and "ligandable" (i.e., and whose physicochemical features – namely, pocket surface and volume as well as balance of electrostatic, hydrophobic and hydrogen bond-forming residues – are suitable to accommodate peptide ligands). Since the target regions of AAVR and A20 are included in the list of ligandable sites, it should not surprise that A20-mimetic peptides interact with multiple sites on all serotypes. At the same time, this also suggests the possibility for smaller A20-mimetic peptides to interact with host cell proteins (HCPs) and other impurities in the feedstock, which reduces their binding selectivity and thwarts their candidacy for experimental evaluation.

Analogous results were observed with AAVR-mimetic sequences. Among them, CVIDGSQSTDDDKIC (A10) and its derivatives A11–A13 featured affinity-like interactions ($|\Delta G_b| \approx 6.5–7.7$ kcal mol^{-1} at pH 7.4) with all target serotypes. In particular, AAV2, AAV5, AAV6, AAV8, and AAV9 formed A10-binding poses that share >90% of paired interactions with AAVR. Once again, shorter variants like A12 and A13 were found to form multiple low-affinity interactions with multiple sites,

TABLE 1 Values of dissociation constant ($K_{D,in\ silico}$) of the complexes formed by A20-mimetic peptides with the capsids of AAV1, AAV2, AAV5, AAV6, AAV8, and AAV9 obtained via molecular docking and dynamics simulations at pH 7.4 and ionic strength of 150 mM and at pH 6.0 and ionic strength of 2 M.

A20-mimetic Sequence	AAV1:peptide $K_{D,in\ silico}$ [M]		AAV2:peptide $K_{D,in\ silico}$ [M]		AAV5:peptide $K_{D,in\ silico}$ [M]		AAV6:peptide $K_{D,in\ silico}$ [M]		AAV8:peptide $K_{D,in\ silico}$ [M]		AAV9:peptide $K_{D,in\ silico}$ [M]	
	pH 6.0	pH 7.4	pH 6.0	pH 7.4	pH 6.0	pH 7.4	pH 6.0	pH 7.4	pH 6.0	pH 7.4	pH 6.0	pH 7.4
CYIHFSGYTNYNPSLKSC (A1)	8.81×10^{-4}	2.16×10^{-6}	7.91×10^{-4}	6.12×10^{-7}	3.83×10^{-3}	1.84×10^{-6}	5.28×10^{-4}	2.54×10^{-7}	4.95×10^{-4}	6.26×10^{-6}	1.27×10^{-4}	6.27×10^{-6}
CYIHFSGYTNYNGSLKSC (A2)	4.88×10^{-4}	1.10×10^{-6}	4.69×10^{-4}	1.07×10^{-6}	4.59×10^{-4}	1.08×10^{-6}	1.04×10^{-4}	1.10×10^{-6}	4.59×10^{-4}	1.03×10^{-6}	4.56×10^{-4}	1.09×10^{-6}
CYVHFSGYSNYSPSC (A3)	1.75×10^{-3}	9.65×10^{-5}	4.27×10^{-4}	7.47×10^{-7}	5.67×10^{-4}	8.58×10^{-6}	4.43×10^{-4}	2.84×10^{-6}	7.47×10^{-5}	4.28×10^{-6}	1.09×10^{-4}	5.41×10^{-5}
CYGHFSGYGNYGPC (A4)	5.70×10^{-4}	2.64×10^{-5}	6.53×10^{-4}	6.17×10^{-6}	1.26×10^{-4}	3.72×10^{-5}	5.26×10^{-4}	1.38×10^{-6}	4.50×10^{-4}	3.44×10^{-6}	2.64×10^{-4}	4.39×10^{-6}
CYGHFSPYGNYGPC (A5)	7.21×10^{-4}	4.18×10^{-5}	7.27×10^{-4}	4.21×10^{-5}	7.77×10^{-4}	4.20×10^{-5}	4.32×10^{-4}	4.36×10^{-5}	7.64×10^{-4}	4.18×10^{-5}	7.34×10^{-4}	4.15×10^{-5}
CYIHFSGYTNYNPC (A6)	8.77×10^{-4}	8.01×10^{-5}	8.27×10^{-4}	1.34×10^{-6}	8.31×10^{-4}	9.12×10^{-5}	4.74×10^{-4}	2.20×10^{-6}	4.06×10^{-4}	3.47×10^{-5}	1.21×10^{-4}	4.56×10^{-5}
CYIHFSPYTNYNPC (A7)	1.09×10^{-4}	6.31×10^{-5}	5.21×10^{-4}	2.45×10^{-5}	9.24×10^{-5}	5.87×10^{-5}	4.01×10^{-5}	2.54×10^{-5}	8.03×10^{-5}	4.60×10^{-5}	1.04×10^{-4}	4.50×10^{-5}
CYHFSYNYPKSC (A8)	5.89×10^{-4}	1.57×10^{-5}	5.99×10^{-4}	1.65×10^{-4}	6.18×10^{-4}	1.72×10^{-5}	1.66×10^{-4}	1.59×10^{-5}	5.79×10^{-4}	1.67×10^{-4}	6.15×10^{-4}	1.59×10^{-5}
CYHFSYNYPC (A9)	6.79×10^{-4}	2.84×10^{-5}	6.61×10^{-4}	2.87×10^{-5}	6.85×10^{-4}	2.94×10^{-5}	2.82×10^{-4}	2.92×10^{-5}	7.03×10^{-4}	2.87×10^{-5}	6.84×10^{-4}	2.98×10^{-5}
A20	†	†	3.68×10^{-7}	9.30×10^{-8}	†	†						

†: not available.

besides the epitopes of A20 and AAVR, suggesting their potential to act as promiscuous, and thus poorly selective, binders.

While the predicted affinity of these sequences was found to be consistently lower than that of A20-mimetics, we note that the binding strength of the AAV:AAVR complexes is originally lower than that of the AAV2:A20 complex. Furthermore, a milder binding strength does not necessarily translate into weaker binding. As noted in prior work,[9] the peptide density on the surface of the resin is sufficient to form multiple interactions with a single capsid, wherein multiple affinity interactions with modest binding energy are synergized into a strong avidity-like binding that efficient AAV capture. The values of peptide density on the resin ($\approx$0.12–0.15 mmol g^{-1}), the resin's specific surface ($\approx$30 m^2 g^{-1}), and the projection area of the triangular unit formed by 3 VPs on the icosahedral capsid ($\approx$81 nm^2) indeed suggest that up to 30 peptides are displayed on pore surface that is impacted by a single capsid, enabling the formation of 3–5 VP:peptide interactions per bound capsid). Finally, moderate binding strength is welcome in the context of affinity purification of AAVs: weak VP:peptide interactions reduce the risk of irreversible adsorption and promote an easier elution of the capsids, thus safeguarding their tissue tropism and transduction activity.

These observations motivate the selection of sequences whose binding energy decreases to $\approx$4–5 kcal mol^{-1} as the pH decreases from pH 7.4 to 6.0 and the ionic strength of the aqueous environment increases to 2 M (representing the transition from the adsorption step conducted in PBS at pH 7.4 to the elution step in 1 M MgCl$_2$ at pH 6.0). This translates in a 120-to-330-fold shift in the dissociation constant for A20-mimetics (K_D, Table 1) and a 30-to-190-fold shift in the K_D of AAVR-mimetics (Table 2). A20-mimetics A1–A4 and AAVR-mimetics A10–A12 are the sequences with the strongest variation in binding energy ($\Delta\Delta G_b$ > 3 kcal mol^{-1}), and thus the highest likelihood of releasing the bound capsids under the desired conditions. The mechanism of VP:peptide dissociation portrayed by the MD simulations is a combined results of the variation in pH and ionic strength. Contrary to what generally observed with peptide ligands, the Coulombic interactions formed by A20 and its mimetics A1–A4 provided a rather minor contribution (11%–15%) to the binding energy at pH 7.4. The only interactions found were formed by cationic Lys in A1 and A2 with Asp514 and Asp 711 on AAV1, Asp269 and Asp 711 on AAV2, Asp704 on AAV5, Asp268 on AAV6, Asp270 on AAV8, and Asp231 on AAV9. Residues A3 and A4 do not contain ionizable residues (except His, which is neutral at pH 7.4). The triplet (DDD) of A10–A12 only targeted Lys508 on AAV1 and AAV2, Lys501 on AAV5, Lys507 on AAV6, and Lys509 on AAV8. Conversely, a strong network of hydrogen bonds and polar interactions formed by the side chains of Ser and Thr, Asn and Gln, His, Asp, and Tyr residues as well as the backbone amide bonds contribute $\approx$65%–74% of the binding energy. Finally, moderate hydrophobic interactions and π-π stacking occur, which account for $\approx$16%–24% of the binding energy.

We also noted that the acidification of the environment to pH 6 causes a minor rearrangement in the capsid structure, together with softening most of the electrostatic interactions. Meanwhile, the addition of MgCl$_2$ – a known chaotrope – destabilizes the electrostatic,

TABLE 2 Values of dissociation constant ($K_{D,in\,silico}$) of the complexes formed by AAVR-mimetic peptides with the capsids of AAV1, AAV2, AAV5, AAV6, AAV8, and AAV9 obtained via molecular docking and dynamics simulations at pH 7.4 and ionic strength of 150 mM and at pH 6.0 and ionic strength of 2 M.

AAVR-mimetic sequence	AAV1:peptide $K_{D,in\,silico}$ [M]		AAV2:peptide $K_{D,in\,silico}$ [M]		AAV5:peptide $K_{D,in\,silico}$ [M]		AAV6:peptide $K_{D,in\,silico}$ [M]		AAV8:peptide $K_{D,in\,silico}$ [M]		AAV9:peptide $K_{D,in\,silico}$ [M]	
	pH 6.0	pH 7.4	pH 6.0	pH 7.4	pH 6.0	pH 7.4	pH 6.0	pH 7.4	pH 6.0	pH 7.4	pH 6.0	pH 7.4
CVIDGSQSTDDDKIC (A10)	3.84×10^{-4}	1.18×10^{-4}	4.66×10^{-4}	4.15×10^{-6}	6.11×10^{-4}	9.83×10^{-6}	5.41×10^{-4}	1.29×10^{-5}	2.21×10^{-4}	8.06×10^{-6}	6.78×10^{-4}	3.08×10^{-6}
CDGSQSTDDDKIC (A11)	3.75×10^{-4}	1.10×10^{-4}	5.31×10^{-4}	2.92×10^{-6}	6.98×10^{-4}	9.90×10^{-5}	4.10×10^{-4}	1.93×10^{-6}	3.28×10^{-4}	7.29×10^{-5}	3.16×10^{-4}	7.97×10^{-6}
CDSQSTDDDKIC (A12)	1.58×10^{-4}	1.29×10^{-4}	5.43×10^{-4}	1.40×10^{-6}	5.71×10^{-4}	9.62×10^{-5}	3.45×10^{-4}	1.56×10^{-6}	2.37×10^{-4}	7.28×10^{-5}	3.52×10^{-4}	8.01×10^{-6}
CSGSTDDDKIC (A13)	9.45×10^{-4}	1.03×10^{-4}	5.80×10^{-4}	1.59×10^{-6}	3.23×10^{-4}	1.24×10^{-5}	3.59×10^{-4}	1.63×10^{-6}	2.06×10^{-4}	7.16×10^{-5}	4.40×10^{-4}	8.56×10^{-6}
GYWIGPFTGGGYIHFSGYT (A14)	3.52×10^{-3}	7.58×10^{-5}	3.81×10^{-4}	7.57×10^{-5}	2.82×10^{-3}	7.26×10^{-5}	2.80×10^{-3}	7.82×10^{-5}	2.80×10^{-3}	7.82×10^{-5}	2.66×10^{-3}	7.78×10^{-5}
GYWIGPFTGPGYIHFSGYT (A15)	6.80×10^{-3}	4.81×10^{-5}	6.37×10^{-3}	4.95×10^{-5}	3.69×10^{-3}	4.98×10^{-5}	3.82×10^{-3}	4.73×10^{-5}	3.84×10^{-3}	4.98×10^{-5}	3.76×10^{-3}	4.74×10^{-5}
GYWIGPFTPGPYIHFSGYT (A16)	3.08×10^{-3}	6.30×10^{-5}	3.23×10^{-3}	6.71×10^{-5}	2.14×10^{-3}	6.61×10^{-5}	2.09×10^{-3}	6.73×10^{-5}	2.22×10^{-3}	6.63×10^{-5}	2.15×10^{-3}	6.38×10^{-5}
LITHPRDYSPKLTPGLYEFG (A17)	4.95×10^{-3}	2.71×10^{-5}	4.70×10^{-3}	2.75×10^{-5}	1.01×10^{-3}	2.74×10^{-5}	9.98×10^{-3}	2.77×10^{-5}	1.02×10^{-3}	2.70×10^{-5}	1.02×10^{-3}	2.72×10^{-5}
AAVR	1.40×10^{-5}	1.80×10^{-6}	1.17×10^{-5}	1.60×10^{-6}	9.01×10^{-6}	1.71×10^{-6}	†	3.57×10^{-6}	1.70×10^{-6}			

†: not available.

hydrophobic, and hydrogen bonding interactions that maintain the native VP conformation and its interaction with the surface-bound peptide ligands. This combination, which triggers the release of the capsids, was observed mostly in the VP:A2, VP:A3, and VP:A10 complexes, whose binding strength at pH 7.4 is moderate ($7.6 > |\Delta G_b| > 6.5$ kcal mol^{-1}) and undergoes the sharpest change upon switching from binding to the elution conditions. For reference, the VP:A20 complex features an in silico $\Delta G_b \approx 8.4$ kcal mol^{-1} and drops by only 1.2 kcal mol^{-1} upon elution. Similarly, the binding strength of AAV:AAVR complexes exhibits no-to-little dependence upon either pH or ionic strength within the explored ranges, and is therefore unlikely to afford sufficient product yield upon mild elution conditions.

In summary, these results support the adoption of small cyclic peptides as ligands for AAV purification via affinity chromatography. As multiple μM-level affinity interactions cooperate into sub-nM avidity capture, peptide-functionalized adsorbents can match their protein-based counterparts in terms of binding capacity and selectivity. Furthermore, small pH variations or additions of chaotropes that disrupt the single VP:peptide interaction are sufficient to trigger capsid release. Conversely, mild elution conditions only marginally affect VP:protein interactions, which require much stronger stimuli, resulting in a loss of yield and transduction activity of the recovered capsids as well as a shorter resin lifetime. Such irreversible multi-site VP:proteins interactions may in fact form a fouling film of bound capsids, which builds up across multiple uses and results in the short lifetime characteristic of commercial adsorbents.

3.2 | Evaluation of AAV binding by the designed peptide ligands in non-competitive mode

The results of molecular docking and dynamics of designed peptides on multiple serotypes delivered a shortlist of sequences – namely, A20-mimetic peptides CYIHFSGYTNYNPSLKSC (A1), CYVHFSGYS-NYSPSC (A3), CYGHFSGYGNYGPC (A4), and CYIHFSGYTNYNPC (A6), and AAVR-mimetic peptides CVIDGSQSTDDDKIC (A10) and CDSQSTDDDKIC (A12) – which were evaluated in dynamic mode against target serotypes AAV1, AAV2, AAV5, AAV6, AAV8, and AAV9. These targets belong to different clones (AAV5) or clades[50,51] – namely A (AAV1 and AAV6), B (AAV2), E (AAV8), and F (AAV9) – with documented therapeutic value. Serotypes 1 and 2 target skeletal, muscle and cardiac cells, and are currently utilized in clinical trials against heart failure, Pompe disease, Hemophilia B, and AAT deficiency.[52] Serotypes 1, 2, 5, 8, 9 target the cells in the central nervous system, especially neurons, and are currently being tested in clinical trials against Alzheimer, Canavan, and Parkinson diseases.[53] Finally, serotype 6 targets epithelial, skeletal cells, and hepatocytes, while serotype 8 targets cardiac cells, skeletal cells, hepatocytes. Notably, affinity resins marketed as serotype-agnostic show excellent binding of AAV1, AAV2, AAV5, and AAV6, but may struggle to capture AAV8 and AAV9, and dedicated adsorbents for their purification have been developed. Accordingly, the model AAVs adopted in this study provide

a broad coverage of the AAV atlas and thus adequate evaluation of the AAV-targeting activity of the designed sequences.

The peptides were conjugated on Toyopearl NH2-750F resin, whose large pore diameter (>100 nm) and small particle size ensures efficient AAV transport into the adsorbent's pores. To evaluate the peptide-based resins under conditions that are representative of biopharmaceutical processes, the feedstocks were formulated as pure AAVs at $\approx 5.0 \times 10^{11}$–$5.0 \times 10^{12}$ vp mL^{-1} in 10 mM Bis-Tris buffer at pH 7.0 and loaded at the ratio of $\approx 10^{13}$ vp mL^{-1} of resin (the expected to be the average binding capacity of the resins). To ensure a stringent evaluation of the performance of peptide-based adsorbents, the bound AAVs were eluted from the peptide-Toyopearl resins under the same conditions adopted for peptide design – namely, 1 M MgCl$_2$ in 10 mM Bis-Tris buffer at pH 6.0. A strong acidic buffer (i.e., 200 mM MgCl$_2$ in 200 mM citrate buffer at pH 2.2 and PBS at pH 2.0, as recommended by the manufacturers) was used for AAV elution from the control POROS™ CaptureSelect™ AAVX and AVB Sepharose HP resins. The values of product loss (i.e., in the flow-through fractions) and yield are summarized in Figure 2.

As shown in Figure 2, the selected peptide resins, and particularly A1-Toyopearl, displayed broad AAV-binding activity. Particularly efficient is the binding of AAV2, which, followed by AAV6, was the serotype most efficiently captured. These results align with the rationale of ligand design, which leverages the known epitopes on AAVR and A20, both of which are AAV2-binding proteins. Among the tested sequences, negligible values of product loss during loading and remarkable values of yield at pH 6.0 were provided by peptides A1 (0.14% and 71.4%, respectively), A4 (0.2% and 61.6%), and A6 (1.36%, 79.7%), which outperformed AAVX POROS™ (1.27% and 63.4%) and AVB Sepharose (0.2%, 45.8%) resins. Notably, the in silico results suggest that the list of binding sites of these peptides include those targeted by AAVR and A20 as well as two epitopes located on VP surface and distant from the VP:VP interface. The availability of neighboring binding sites promotes capsid capture, translating in higher values of capacity and lower loss during loading. At the same time, the significant drop in binding strength upon mild acidification is coherent with the excellent values of product recovery. The propensity of AAV2 to aggregate into soluble multimeric constructs may also promote the formation of multi-site interactions with the peptide-functionalized surface, and thus the efficient capture of this serotype.

Efficient binding and recovery were also observed with AAV1, AAV6, and AAV8. In particular, peptides A1 and A4 afforded excellent binding and gentle release of AAV1 and AAV6. The values of product yield were respectively 66.2% and 54.1% with A1-Toyopearl resin, which performed comparably to AAVX POROS™ resin (74.8% and 67.4%) and outperformed AVB Sepharose (55.5% and 15.0%); and 43.9% and 49.6% with A4-Toyopearl resin. Both serotypes belong to Clade A, which is closely related to Clade B, to which AAV2 belongs. AAV1 and AAV6 feature, in fact, a 91%–92% structural homology with AAV2 (*note*: sequence homology, however, is 81%–83%).[51] With structural complementarity playing a key role in AAV docking on the peptide-functionalized surface, it stands to reason that structural
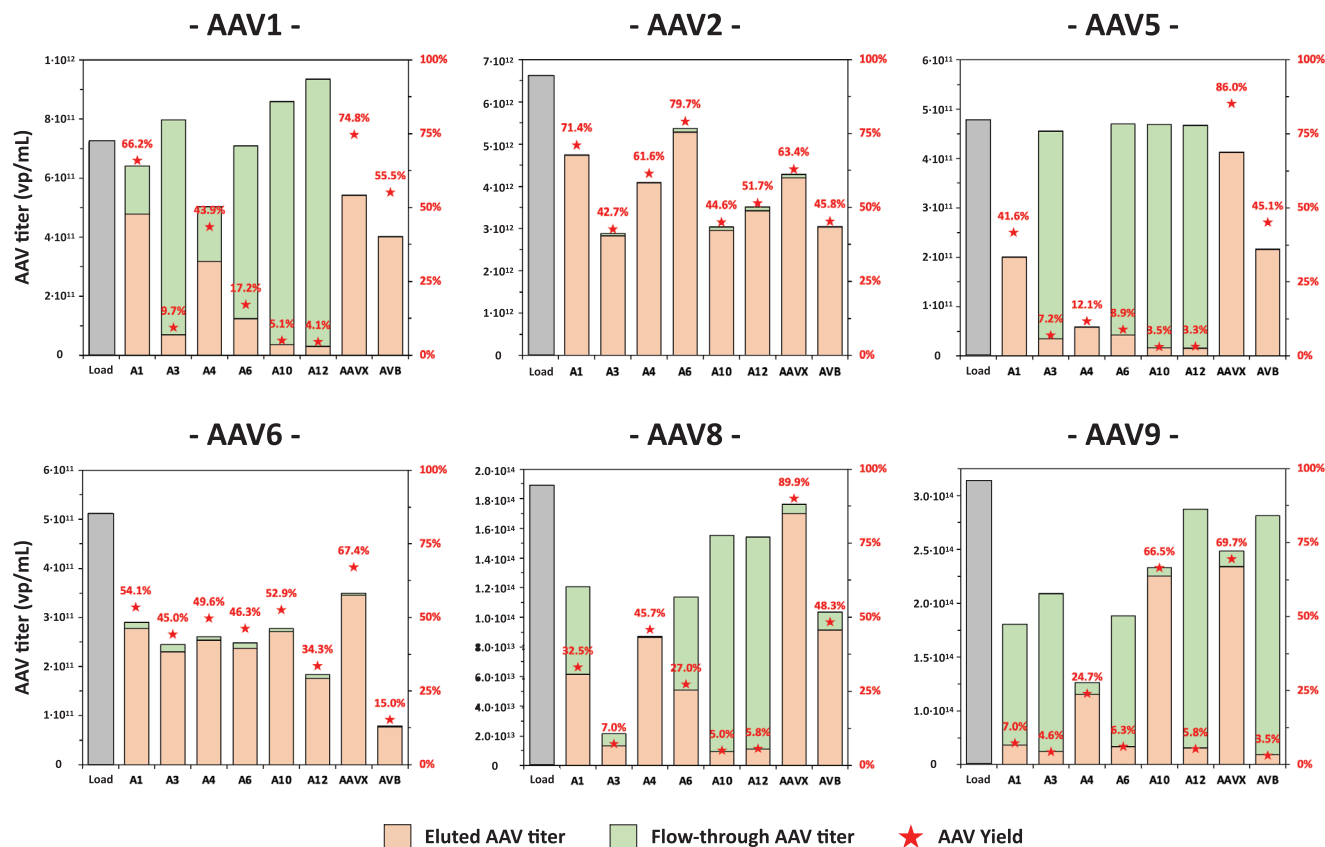
FIGURE 2 Values of titer in the flow-through and wash fractions (green), titer in the elution fractions (orange), and yield (red stars) of AAV1, AAV2, AAV5, AAV6, AAV8, and AAV9 obtained via bind-and-elute studies in non-competitive mode using peptide-based resins (A1) CYIHFSGYTNYNPSLKSC-, (A3) CYVHFSGYSNYSPSC-, (A4) CYGHFSGYGNYGPC-, (A6) CYIHFSGYTNYNPC-, (A10) CVIDGSQSTDDDKIC-, and (A12) CDSQSTDDDKIC-Toyopearl resins, and control adsorbents POROS™ CaptureSelect™ AAVX (AAVX) and AVB Sepharose HP (AVB) resins. The AAV titer in the flow-through, wash, and elution fractions was measured using serotype-specific ELISA kits.

homology is an underlying factor of AAV1, AAV2, and AAV6 binding shared by these three sequences.

Peptides A1 and A4 also showed a similar performance with AAV8, affording product yield of 32.5% and 45.7% respectively, followed by A6 with 27%. Notably, AA8 (Clade E) exhibits a 94% structural homology, but only 82% sequence homology, with AAV2.[51] When tested against AAV9, however, only A4 maintained acceptable product recognition, with only 4.2% loss and 24.7% yield. Conversely, A1 only afforded 7% yield and significant product loss. Notably, A10 returned a remarkable yield of 66.5%, comparable with that of AAVX POROS™ resin (69.7%) and significantly higher than that of AVB Sepharose resin (3.5%).

As anticipated, the capture of AAV5 proved the most challenging: the most unique among all AAVs, AAV5 exhibits a poor structural (58%–71%) and sequence (58%–79%) homology with the other serotypes evaluated in this study.[51] It is therefore remarkable that peptide A1 captured (0.2% loss) and released it efficiently (41.6% yield).

Three general conclusions can be drawn from the experimental evaluation of the in silico-selected peptides. First, peptide CYGHFS-GYGNYGPC (A4) performed well with all serotypes, exhibiting neg-

ligible product loss, suggesting that the variations in yield should be attributed to differences in binding strength to the various serotypes. A comparative evaluation of the values of K_D measured in silico (Table 1) and the amounts of eluted AAVs show that high yields (45%–80%) were obtained when a >100-fold increase in K_D was registered (AAV2, AV6, and AAV8), whereas moderate yields (25%–44%) were obtained when only a 10-to-50 fold increase was registered (AAV1 and AAV9). Finally, the lowest yield, obtained with AAV5, coincided with a mere 3-fold increase in K_D. A similar comparison can be made for CYIHF-SGYTNYNPSLKSC (A1), whose high yield of AAV1, AAV2, and AAV6 coincided respectively with a 400-, 130-, and 2080-fold increase in K_D, whereas the product loss and lower yield registered with AAV8 and AAV9 coincided with both a lower binding strength and a lower shift in K_D. Shifts in affinity of such magnitude under mild acidification (pH 6) are hardly attainable with protein ligands, which require much harsher environments to release the bound capsids, and justify the choice of peptide ligands for the purification of labile products such as viral vectors.

Secondly, peptides A3, A6, and A12 behaved differently with different serotypes, affording excellent capture and yield of AAV2 and AAV6, but high product loss and consequently low yield of AAV1,

AAV5, AAV8, and AAV9. Notably, the low capture of these serotypes is matched by the *in silico* results, which predicted a low binding strength of these peptides at pH 7.4 ($K_D > 3.5 \times 10^{-5}$ M); conversely, a higher binding strength ($K_D \approx 7.5 \times 10^{-7}$ M–2.8×10^{-6} M) was predicted for AAV2 and AAV6, suggesting that, while moderate affinity is still desirable, binding strength must be above a minimum threshold to ensure sufficient product capture. On the other hand, the serotypes that were poorly captured by A3, A6, and A12 were effectively recovered by A1 and A4, thus prompting the choice of discontinue these peptides.

Thirdly, sequence CVIDGSQSTDDDKIC (A10) performed uniquely well with AAV9, on par with AAVX POROS™ resin, outperforming all other peptide-based resins and AVB Sepharose. Once again, the performance of the peptide is inscribed in the values of binding strength at pH 7.4 ($K_D \approx 3.08 \times 10^{-6}$ M) and strong affinity loss (220-fold increase in K_D) upon acidification predicted in silico. Under the light of these results, peptides A1, A4, and A10 were carried forward for additional experimental evaluation.

3.3 | Purification of AAV2 from HEK293 and Sf9 cell lysates

We proceeded to evaluate the selected peptide-based adsorbents A1-, A4-, and A10-Toyopearl resin by purifying AAV2 from a clarified HEK293 cell culture lysate. The HEK293 cell lysate (AAV2 titer $\approx 1.9 \times 10^{12}$ vp mL^{-1}; HCP titer ≈ 0.3 mg mL^{-1}) and the Sf9 cell lysate (AAV2 titer $\approx 1.56 \times 10^{12}$ vp mL; HCP titer ≈ 1.1 mg mL^{-1}) were prepared via triple transfection and baculovirus infection, respectively, following the protocols described in the literature.[11,54,55–58] Similarly, a residence time (RT) of 3 min for both binding and washing steps was adopted based on industrial operating conditions. The chromatograms of AAV2 purification are presented in Figure S3, while the analysis of the collected fractions via size exclusion (SEC) and steric exclusion chromatography (SXC) are reported in Figures S4 and S5. Finally, the resulting values of AAV2 yield and logarithmic removal of HEK293 host cell proteins (HCP LRV) from the HEK293 and Sf9 feedstocks are summarized in Figure 3A,B respectively.

The results of AAV2 purification from the HEK293 cell lysate (Figure 3A) mirror the values obtained in non-competitive conditions in Figure 2B. Little-to-no product loss was observed in the flow-through and wash fractions, confirming that the peptides maintain a strong AAV biorecognition when loaded with complex feedstocks. The product yields, ranging between 30% (A4- and A6-Toyopearl resins) and 78% (A1-Toyopearl resins), were either on par with or substantially higher than those returned by the reference POROS™ CaptureSelect™ AAVX Affinity and AVB Sepharose HP resins. Finally, the values of HCP LRV were consistently above 2, reaching values as high as 2.86, corresponding to a >720-fold decrease of protein contaminants, thus matching the reference adsorbents in terms of product purity as well. The analysis of the feedstock and elution fractions via size exclusion chromatography (SEC, Figure S4) and steric exclusion chromatography (SXC, Figure S5) offer a clear view of the purification performance of the selected resins. While HEK293 ELISA assays returns the titer of

HCPs only, analytical chromatography provides a quantitative measure of all process-related impurities (e.g., denatured or hydrolyzed HCPs, other non-proteinaceous metabolites, host cell DNA and RNA, and media components) as well as product-related impurities (e.g., capsid fragments). Echoing the ELISA results, the SEC and SXC results demonstrate the high purity of the AAV2 eluted from the peptide-based adsorbents. Specifically, the comparative analysis of the SEC chromatograms returns global values of impurity decrease of 150-fold for A1-Toyopearl resin, 730-fold for A4-Toyopearl resin, and 550-fold for A10-Toyopearl resin. The SXC chromatograms provided similar results, confirming that peptide-based adsorbents deliver eluates whose purity is comparable to that afforded by the affinity adsorbents utilized in the gene therapy industry.

Excellent results were also obtained on the front of AAV2 purification from the Sf9 cell lysate (Figure 3B). As observed before, A1-Toyopearl resin afforded the highest product yield (70%), although the purity of the eluate was somewhat wanting, whereas A4- and A10-Toyopearl resin performed comparably to the control resins. It is possible that the association of some HCPs to the AAV2 capsids is responsible for the lower purity of the A1 eluates. The titer of HEK293 and Sf9 HCPs in the A1 *vs.* AAVX eluates differ by 9.7 and 13.7 μg mL^{-1}, respectively, corresponding to 2.7% and 1.2% of the HCPs in the feedstocks. We can also expect that A1, as a small peptide ligand, does not match the binding selectivity of its V_HH counterparts. This can be alleviated by decreasing the density of A1 on the surface of the resin or by further optimizing its sequence, which will be the object of future studies. We should also note that, unlike the HEK293 cell lysate, the Sf9 harvest features a significantly higher HCP titer (0.3 vs. 1.1 mg mL^{-1}, respectively), which explains why the values of HCP LRV are lower than those reported in Figure 3A. Nonetheless, the concentration of residual HCPs in the eluates from the peptide-based adsorbents were consistently below 35 μg mL^{-1}, in line with eluates of affinity resins characteristic of chromatographic processes for biotherapeutics.

The purification performance of the peptide-based adsorbents is particularly remarkable when considering that elution is conducted under near-physiological pH. To quantify the benefits of mild elution, we conducted a comparative measurement of the transduction activity on human epithelial cells (HT1080) of the AAV2 isolated from HEK293 cell culture lysate using A1-, A4-, and A10-Toyopearl resins vs. POROS™ CaptureSelect™ AAVX resin (*note*: the gene encapsidated in the target AAV2 encodes for green fluorescence protein (GFP), which enables quantifying the transduction activity via fluorescence flow cytometry). The transduction activity (i.e., the ability of a virus to effectively deliver its gene payload to the target cells) is a critical quality parameter of viral vectors and is significantly impacted by the process parameters. AAVs, like most viral vectors, are prone to lose their activity in response to variations in buffer conductivity and pH used to control adsorption and elution during chromatographic purification. Current affinity resins, however, require a rather acidic elution pH, in the range ≈ 2–3 depending upon serotype and desired elution yield (>50%), to achieve sufficient product yield. By enabling elution under significantly milder conditions (pH 6.0), peptide-based adsorbents are expected to return products with higher activity than their
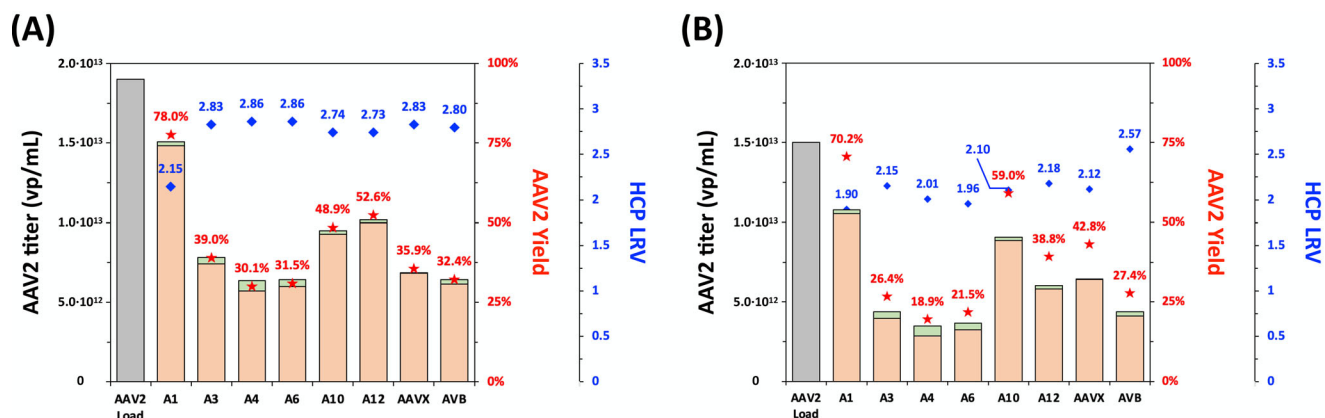
FIGURE 3 Values of AAV2 titer in the flow-through and wash fractions (green histograms), AAV2 titer in the elution fractions (orange histograms), AAV2 yield (red stars), and logarithmic removal of HCPs (HCP LRV, blue diamonds) obtained via chromatographic purification of AAV2 from (A) a clarified HEK293 cell lysate (AAV2 titer: $\approx 1.9 \times 10^{12}$ vp mL^{-1}; HCP titer: ≈ 0.3 mg mL^{-1}) and (B) a clarified Sf9 cell lysate (AAV2 titer: $\approx 1.56 \times 10^{12}$ vp mL^{-1}; HCP titer: ≈ 1.1 mg mL^{-1}) using adsorbents (A1) CYIHFSGYTNYNPSLKS-, (A4) CYGHFSGYGNYGPC-, and (A10) CVIDGSQSTDDDKIC-Toyopearl resins together with control adsorbents POROS™ CaptureSelect™ AAVX (AAVX) and AVB Sepharose HP (AVB) resins. The AAV titer in the flow-through, wash, and elution fractions was measured using serotype-specific ELISA kits.
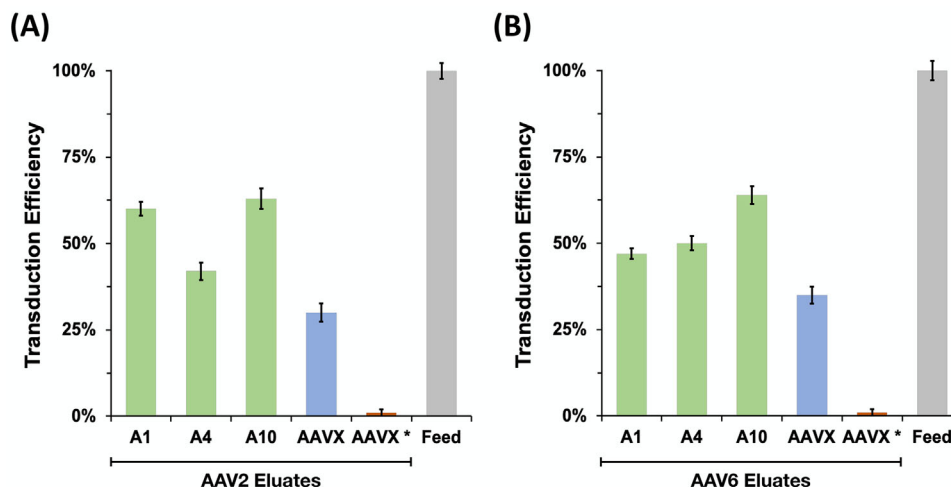
FIGURE 4 Values of relative transduction efficiency of (A) AAV2 and (B) AAV6 purified from clarified HEK293 cell lysates using peptide-based adsorbents (A1) CYIHFSGYTNYNPSLKS-, (A4) CYGHFSGYGNYGPC-, and (A10) CVIDGSQSTDDDKIC-Toyopearl resins together with control adsorbent POROS™ CaptureSelect™ AAVX resin (note: AAVX and AAVX* denote the eluate that was neutralized respectively immediately and 48 h after collection). The transduction efficiency (TU/vp) of eluted AAVs was measured on human epithelial (HT1080; 10^7 vp per cell) by performing a green fluorescence assay using a CytoFLEX Flow Cytometer. The values of relative transduction efficiency were calculated as the ratio of transduction efficiency of eluted AAVs vs. fed AAVs (Equation 2). The corresponding flow cytometry plots are reported in Figures S7–S14, while the resulting values of transduction efficiency are listed in Table S3.

commercial counterparts. The values in Figure 4 confirm this hypothesis, showing that the activity of AAV2 and AAV6 eluted at pH 6 is between 1.5- and 2.2-fold higher than those isolated by the POROS™ AAVX resin. Particularly remarkable is the activity of the AAV2 and AAV6 purified using the A10-Toyopearl resins, which – respectively at 62% and 63% transduction relative to the AAVs in the corresponding feedstocks – match the values obtained via CsCl and iodixanol gradient ultracentrifugation.[11,54] In this context, we note that the peptide-based resins release mostly intact and gene-loaded AAV particles, showing no signs of capsid fragmentation or aggregation (Figure S6).

3.4 | Dynamic AAV binding capacity and reusability of peptide-based adsorbents in competitive mode

Two additional performance parameters determine the suitability of an affinity resin for industrial biopharmaceutical manufacturing: the dynamic binding capacity at 10% product breakthrough (DBC$_{10\%}$) and the reusability upon subsequent cleaning in place. Accordingly, we measured the DBC$_{10\%}$ of (A1) CYIHFSGYTNYNPSLKS-, (A4) CYGHFSGYGNYGPC-, and (A10) CVIDGSQSTDDDKIC-Toyopearl resins via frontal loading of a clarified lysate containing AAV2 at the

TABLE 3 Values of dynamic AAV2 binding capacity ($DBC_{10\%}$) of peptide-functionalized resins loaded (RT: 3 min) with a clarified HEK293 cell lysate containing AAV2 at the titer of 2.51×10^{12} vp mL^{-1}. – -: not available.

Resin	$DBC_{10\%}$ [vp AAV per mL of resin]	
	Cycle 1	Cycle 20
A1-Toyopearl	2.80×10^{14}	2.35×10^{14}
A4-Toyopearl	2.52×10^{14}	2.16×10^{14}
A10 -Toyopearl	2.10×10^{14}	2.01×10^{14}
POROS™ AAVX	5.60×10^{14}	- -

titer of 2.51×10^{12} vp mL^{-1} at the residence time (RT) of 3 min. The clarified lysate was adopted in lieu of a pure AAV2 solution to provide a realistic evaluation of the binding capacity of the resins, whose operation is intended for competitive conditions. The adopted RT is recommended for POROS™ AAVX and AVB Sepharose resins and was therefore adopted to ensure comparability.

The values of $DBC_{10\%}$, compared in Table 3, demonstrate that the peptide-based adsorbents, notwithstanding the milder binding strength, feature an AAV binding capacity on par with or exceeding that of commercial affinity resins. This can be ascribed to the multi-site interaction governing the AAV adsorption by the peptide-functionalized surface, whose effective binding strength matches that of protein-functionalized adsorbents. This decouples the value of binding capacity from the single AAV:peptide binding strength and makes it mostly – or solely – dependent on the specific surface of the resin.

Secondly, the binding capacity and selectivity of an affinity resin can decrease over time due to several factors, such as chemical degradation, physical damage, and fouling, leading to a loss of product yield and purity as well as additional costs related to the replacement and validation of the adsorbent. Unlike Protein A-based resins for antibody purification, whose lifetime has now reached 150–200 cycles with intermediate caustic cleaning in place, commercial affinity resins for AAV purification are not designed to withstand harsh alkaline treatment and rapidly lose their binding capacity, mandating frequent column replacement (*note*: the manufacturers recommend cleaning the resins with aqueous NaOH at concentration below 25 mM). We therefore evaluated the reusability of the peptide-based adsorbents to withstand 20 cycles of AAV2 purification followed by regeneration and cleaning in place. As shown in Table 3, A1-, A4-, and A10-Toyopearl resins consistently maintained their $DBC_{10\%}$ ($\approx$10% variation), demonstrating the chemical stability of the selected peptides and their linkage to the resin.

4 | CONCLUSIONS

Viral vectors are rapidly becoming – and will soon be – an integral part of modern medicine: as the discourse on biomanufacturing evolves (e.g., the layout of platform processes, whether scaling-up vs.

scaling-out will meet the growing demand, or the standardization and comparability in the process analytical technology, etc.), the need of a portfolio of bioprocess technologies dedicated to the expression, purification, and analytical characterization of viral vectors becomes every day more evident. Contributing to the efforts on improving downstream technologies, this study presents an ensemble of small peptide affinity ligands designed to transform AAV purification as they provide (i) selective as well as flexible product capture, being serotype-agnostic and applicable to both HEK293 and Sf9 fluids; (ii) gentle elution, allowing product release under near-physiological pH; and (iii) robust reusability, maintaining a high binding capacity over multiple purification cycles. Furthermore, unlike affinity adsorbents that rely on antibody-derived ligands, the proposed adsorbents are undoubtedly more scalable and affordable, and they leverage the ability to mass manufacture GMP-quality peptides at relatively low cost ($\approx$US$8 per gram per amino acid residue, when manufactured at >10 kg scale per year).[59,60] Combining the cost of synthesis with the average values of number of residues ($\approx$15–17) and molecular weight ($\approx$1.5–1.7 kg mol^{-1}) of the peptide ligands, their density on the resin surface ($\approx$0.03 mol per liter), and the cost of the base resin ($\approx$\$2500 per liter) indicates that direct material cost of the peptide-functionalized adsorbent ranges between \$7900 and \$9500 per liter, when produced at the $\approx$100 L scale (*note*: direct labor and manufacturing overhead are not factored). These considerations, combined with the purification performance of peptide-functionalized adsorbents presented by our team and by several others in the literature,[9,11,55–58,61–65] show the promise of this technology to transform the biomanufacturing of modern medicines and reduce their cost (*note*: the latter is of particular concern, given the price tag of gene therapies well above US$1M per patient). Under the light of these considerations, our team plans to demonstrate further the technology introduced in this study by purifying AAVs of different serotypes from a variety of HEK293 and Sf9 fluids. We also intend to leverage the in silico-in vitro toolbox for ligand development to establish a portfolio of peptide-based purification tools for the other key viral vector families, namely lentivirus (LV), adenovirus (Ad), and baculovirus (BV).

AUTHOR CONTRIBUTIONS

Shriarjun Shastry, Wenning Chu, Eduardo Barbieri, Paul Greback-Clarke, William K. Smith, Christopher Cummings, and Arianna Minzoni conducted the experimental work. Jennifer Pancorbo, Gary Gilleskie, Kimberly Ritola, Michael A. Daniele, Thomas F. Johnson, and Stefano Menegatti conceived the work and wrote the manuscript.

CONFLICT OF INTEREST STATEMENT

DATA AVAILABILITY STATEMENT

ORCID

Wenning Chu https://orcid.org/0000-0002-6033-0963
Stefano Menegatti https://orcid.org/0000-0001-5633-434X

REFERENCES

1. Bulcha, J. T., Wang, Y., Ma, H., Tai, P. W. L., & Gao, G. (2021). Viral vector platforms within the gene therapy landscape. *Signal Transduction and Targeted Therapy*, 6(1), 53. https://doi.org/10.1038/s41392-021-00487-6

2. Fukuhara, H., Ino, Y., & Todo, T. (2016). Oncolytic virus therapy: A new era of cancer treatment at dawn. *Cancer Science*, 107(10), 1373–1379. https://doi.org/10.1111/cas.13027

3. Rodrigues, A. F., Soares, H. R., Guerreiro, M. R., Alves, P. M., & Coroadinha, A. S. (2015). Viral vaccines and their manufacturing cell substrates: New trends and designs in modern vaccinology. *Biotechnology Journal*, 10(9), 1329–1344. https://doi.org/10.1002/biot.201400387

4. Zaidi, S. S. A., & Mansoor, S. (2017). Viral vectors for plant genome engineering. *Frontiers in Plant Science*, 8, 539–545. https://www.frontiersin.org/articles/10.3389/fpls.2017.00539

5. Chandler, R. J., Sands, M. S., & Venditti, C. P. (2017). Recombinant adeno-associated viral integration and genotoxicity: Insights from animal models. *Human Gene Therapy*, 28(4), 314–322. https://doi.org/10.1089/hum.2017.009

6. Verdera, H. C., Kuranda, K., & Mingozzi, F. (2020). AAV vector immunogenicity in humans: A long journey to successful gene transfer. *Molecular Therapy*, 28(3), 723–746. https://doi.org/10.1016/j.ymthe.2019.12.010

7. Ura, T., Okuda, K., & Shimada, M. (2014). Developments in viral vector-based vaccines. *Vaccines*, 2(3), 624–641. https://doi.org/10.3390/vaccines2030624

8. Terova, O., Soltys, S., Hermans, P., de Rooij, J., & Detmers, F. (2018). Overcoming downstream purification challenges for viral vector manufacturing: Enabling advancement of gene therapies in the clinic. *Cell and Gene Therapy Insights*, 4, 101–111. https://doi.org/10.18609/cgti.2018.017

9. Chu, W., Shastry, S., Barbieri, E., Prodromou, R., Greback-Clarke, P., Smith, W., Moore, B., Kilgore, R., Cummings, C., Pancorbo, J., Gilleskie, G., Daniele, M. A., & Menegatti, S. (2023). Peptide ligands for the affinity purification of adeno-associated viruses from HEK 293 cell lysates. *Biotechnology and Bioengineering*, 120(8), 2283–2300. https://doi.org/10.1002/bit.28495

10. Łącki, K. M., & Riske, F. J. (2020). Affinity chromatography: An enabling technology for large-scale bioprocessing. *Biotechnology Journal*, 15(1), 1800397. https://doi.org/10.1002/biot.201800397

11. Florea, M., Nicolaou, F., Pacouret, S., Zinn, E. M., Sanmiguel, J., Andres-Mateos, E., Unzu, C., Wagers, A. J., & Vandenberghe, L. H. (2023). High-efficiency purification of divergent AAV serotypes using AAVX affinity chromatography. *Molecular Therapy – Methods & Clinical Development*, 28, 146–159. https://doi.org/10.1016/j.omtm.2022.12.009

12. Adams, B., Bak, H., & Tustian, A. D. (2020). Moving from the bench towards a large scale, industrial platform process for adeno-associated viral vector purification. *Biotechnology and Bioengineering*, 117(10), 3199–3211. https://doi.org/10.1002/bit.27472

13. Kilgore, R., Chu, W., Bhandari, D., Fischler, D., Carbonell, R. G., Crapanzano, M., & Menegatti, S. (2023). Development of peptide affinity ligands for the purification of polyclonal and monoclonal Fabs from recombinant fluids. *Journal of Chromatography A*, 1687, 463701. https://doi.org/10.1016/j.chroma.2022.463701

14. Xiao, X., Kilgore, R., Sarma, S., Chu, W., Menegatti, S., & Hall, C. K. (2022). De novo discovery of peptide-based affinity ligands for the fab fragment of human immunoglobulin G. *Journal of Chromatography A*, 1669, 462941. https://doi.org/10.1016/j.chroma.2022.462941

15. Chu, W., Sripada, S. A., Reese, H. R., Bhandari, D., Adams, A., Sly, J., Crapanzano, M., & Menegatti, S. (2021). Purification of polyclonal immunoglobulin G from human serum using peptide-based adsorbents. *AIChE Journal*, 67(12), e17482. https://doi.org/10.1002/aic.17482

16. Chu, W., Prodromou, R., Day, K. N., Schneible, J. D., Bacon, K. B., Bowen, J. D., Kilgore, R. E., Catella, C. M., Moore, B. D., Mabe, M. D., Alashoor, K., Xu, Y., Xiao, Y., & Menegatti, S. (2021). Peptides and pseudopeptide ligands: A powerful toolbox for the affinity purification of current and next-generation biotherapeutics. *Journal of Chromatography A*, 1635, 461632. https://doi.org/10.1016/j.chroma.2020.461632

17. Chu, W., Prodromou, R., Moore, B., Elhanafi, D., Kilgore, R., Shastry, S., & Menegatti, S. (2022). Development of peptide ligands for the purification of α-1 antitrypsin from cell culture fluids. *Journal of Chromatography A*, 1679, 463363. https://doi.org/10.1016/j.chroma.2022.463363

18. Prodromou, R., Day, K. N., Saberi-Bosari, S., Schneible, J. D., Mabe, M. D., San Miguel, A., Daniele, M. A., Pozdin, V., & Menegatti, S. (2021). Engineering next generation cyclized peptide ligands for light-controlled capture and release of therapeutic proteins. *Advanced Functional Materials*, 31(27), 2101410. https://doi.org/10.1002/adfm.202101410

19. Prodromou, R., Moore, B. D., Chu, W., Deal, H., San Miguel, A., Brown, A. C., Daniele, M. A. A., Pozdin, V. A., & Menegatti, S. (2023). Molecular engineering of cyclic azobenzene-peptide hybrid ligands for the purification of human blood factor VIII via photo-affinity chromatography. *Advanced Functional Materials*, n/a(n/a), 2213881. https://doi.org/10.1002/adfm.202213881

20. Brennan, T. A., & Wilson, J. M. (2014). The special case of gene therapy pricing. *Nature Biotechnology*, 32(9), 874–876. https://doi.org/10.1038/nbt.3003

21. Hanwell, M. D., Curtis, D. E., Lonie, D. C., Vandermeersch, T., Zurek, E., & Hutchison, G. R. (2012). Avogadro: An advanced semantic chemical editor, visualization, and analysis platform. *Journal of Cheminformatics*, 4(1), 17. https://doi.org/10.1186/1758-2946-4-17

22. Schmid, N., Eichenberger, A. P., Choutko, A., Riniker, S., Winger, M., Mark, A. E., & van Gunsteren, W. F. (2011). Definition and testing of the GROMOS force-field versions 54A7 and 54B7. *European Biophysics Journal*, 40(7), 843–856. https://doi.org/10.1007/s00249-011-0700-9

23. Ke, Q., Gong, X., Liao, S., Duan, C., & Li, L. (2022). Effects of thermostats/barostats on physical properties of liquids by molecular dynamics simulations. *Journal of Molecular Liquids*, 365, 120116. https://doi.org/10.1016/j.molliq.2022.120116

24. Singhal, A., Schneible, J. D., Lilova, R. L., Hall, C. K., Menegatti, S., & Grafmüller, A. (2020). A multiscale coarse-grained model to predict the molecular architecture and drug transport properties of modified chitosan hydrogels. *Soft Matter*, 16(47), 10591–10610. https://doi.org/10.1039/D0SM01243B

25. Schneible, J. D., Shi, K., Young, A. T., Ramesh, S., He, N., Dowdey, C. E., Dubnansky, J. M., Lilova, R. L., Gao, W., Santiso, E., Daniele, M., & Menegatti, S. (2020). Modified gaphene oxide (GO) particles in peptide hydrogels: A hybrid system enabling scheduled delivery of synergistic combinations of chemotherapeutics. *Journal of Materials Chemistry B*, 8(17), 3852–3868. https://doi.org/10.1039/D0TB00064G

26. Schneible, J. D., Singhal, A., Lilova, R. L., Hall, C. K., Grafmüller, A., & Menegatti, S. (2019). Tailoring the chemical modification of chitosan hydrogels to fine-tune the release of a synergistic combination of chemotherapeutics. *Biomacromolecules, 20*(8), 3126–3141. https://doi.org/10.1021/acs.biomac.9b00707

27. Kish, W. S., Sachi, H., Naik, A. D., Roach, M. K., Bobay, B. G., Blackburn, R. K., Menegatti, S., & Carbonell, R. G. (2017). Design, selection, and development of cyclic peptide ligands for human erythropoietin. *Journal of Chromatography A, 1500*, 105–120. https://doi.org/10.1007/s10822-013-9644-8

28. Bas, D. C., Rogers, D. M., & Jensen, J. H. (2008). Very fast prediction and rationalization of pKa values for protein-ligand complexes. *Proteins: Structure, Function, and Bioinformatics, 73*(3), 765–783. https://doi.org/10.1002/prot.22102

29. Honorato, R. V., Koukos, P. I., Jiménez-García, B., Tsaregorodtsev, A., Verlato, M., Giachetti, A., Rosato, A., & Bonvin, A. M. J. J. (2021). Structural biology in the clouds: The WeNMR-EOSC ecosystem. *Frontiers in Molecular Biosciences, 8*, https://www.frontiersin.org/articles/10.3389/fmolb.2021.729513

30. van Zundert, G. C. P., Rodrigues, J. P. G. L. M., Trellet, M., Schmitz, C., Kastritis, P. L., Karaca, E., Melquiond, A. S. J., van Dijk, M., de Vries, S. J., & Bonvin, A. M. J. J. (2016). The HADDOCK2.2 Web Server: User-friendly integrative modeling of biomolecular complexes. *Computation Resources for Molecular Biology, 428*(4), 720–725. https://doi.org/10.1016/j.jmb.2015.09.014

31. Spiliotopoulos, D., Kastritis, P. L., Melquiond, A. S. J., Bonvin, A. M. J. J., Musco, G., Rocchia, W., & Spitaleri, A. (2016). DMM-PBSA: A new HADDOCK scoring function for protein-peptide docking. *Frontiers in Molecular Biosciences, 3*, 46–59. https://www.frontiersin.org/articles/10.3389/fmolb.2016.00046

32. Gregorevic, P., Blankinship, M. J., Allen, J. M., Crawford, R. W., Meuse, L., Miller, D. G., Russell, D. W., & Chamberlain, J. S. (2004). Systemic delivery of genes to striated muscles using adeno-associated viral vectors. *Nature Medicine, 10*(8), 828–834. https://doi.org/10.1038/nm1085

33. Velez-Fort, M., Bracey, E. F., Keshavarzi, S., Rousseau, C. V., Cossell, L., Lenzi, S. C., Strom, M., & Margrie, T. W. (2018). A circuit for integration of head- and visual-motion signals in layer 6 of mouse primary visual cortex. *Neuron, 98*(1), 179–191. https://doi.org/10.1016/j.neuron.2018.02.023

34. Sirika, P., Wei, Z., Fang, C., Puschnik Andreas, S., Meyer Nancy, L., Ganaie Safder, S., Xuefeng, D., Wosen Jonathan, E., Omar, D., Ziying, Y., Engelhardt John, F., Brown Kevin, E., Chapman Michael, S., Jianming, Q., & Carette Jan, E. (2017). Adeno-associated Virus (AAV) serotypes have distinctive interactions with domains of the cellular AAV receptor. *Journal of Virology, 91*(18), e00391–e00417. https://doi.org/10.1128/JVI.00391-17

35. Meyer, N. L., & Chapman, M. S. (2022). Adeno-associated virus (AAV) cell entry: Structural insights. *Trends in Microbiology, 30*(5), 432–451. https://doi.org/10.1016/j.tim.2021.09.005

36. Summerford, C., Bartlett, J. S., & Samulski, R. J. (1999). αVβ5 integrin: A co-receptor for adeno-associated virus type 2 infection. *Nature Medicine, 5*(1), 78–82. https://doi.org/10.1038/4768

37. Qing, K., Mah, C., Hansen, J., Zhou, S., Dwarki, V., & Srivastava, A. (1999). Human fibroblast growth factor receptor 1 is a co-receptor for infection by adeno-associated virus 2. *Nature Medicine, 5*(1), 71–77. https://doi.org/10.1038/4758

38. Aravind, A., Hamra Julie, B., Lakshmanan, G., Agbandje-McKenna, M., & Samulski Richard, J. (2006). Adeno-associated virus type 2 contains an integrin α5β1 binding domain essential for viral cell entry. *Journal of Virology, 80*(18), 8961–8969. https://doi.org/10.1128/JVI.00843-06

39. Bassel, A., Dirk, G., Kusum, P., Yant Stephen, R., Hui, X., & Kay Mark, A. (2006). The 37/67-kilodalton laminin receptor is a receptor for adeno-associated virus serotypes 8, 2, 3, and 9. *Journal of Virology, 80*(19), 9831–9836. https://doi.org/10.1128/JVI.00878-06

40. Blackburn, S. D., Steadman, R. A., & Johnson, F. B. (2006). Attachment of adeno-associated virus type 3H to fibroblast growth factor receptor 1. *Archives of Virology, 151*(3), 617–623. https://doi.org/10.1007/s00705-005-0650-6

41. Ling, C., Lu, Y., Kalsi, J. K., Jayandharan, G. R., Li, B., Ma, W., Cheng, B., Gee, S. W. Y., McGoogan, K. E., Govindasamy, L., Zhong, L., Agbandje-McKenna, M., & Srivastava, A. (2010). Human hepatocyte growth factor receptor is a cellular coreceptor for adeno-associated virus serotype 3. *Human Gene Therapy, 21*(12), 1741–1747. https://doi.org/10.1089/hum.2010.075

42. Pasquale, G. D., Davidson, B. L., Stein, C. S., Martins, I., Scudiero, D., Monks, A., & Chiorini, J. A. (2003). Identification of PDGFR as a receptor for AAV-5 transduction. *Nature Medicine, 9*(10), 1306–1312. https://doi.org/10.1038/nm929

43. Day, K., Prodromou, R., Saberi Bosari, S., Lavoie, A., Omary, M., Market, C., San Miguel, A., & Menegatti, S. (2019). Discovery and evaluation of peptide ligands for selective adsorption and release of Cas9 nuclease on solid substrates. *Bioconjugate Chemistry, 30*(12), 3057–3068. https://doi.org/10.1021/acs.bioconjchem.9b00703

44. Barozzi, A., Lavoie, R. A., Day, K. N., Prodromou, R., & Menegatti, S. (2020). Affibody-binding ligands. *International Journal of Molecular Sciences, 21*(11). https://doi.org/10.3390/ijms21113769

45. Bowen, J., Schneible, J., Bacon, K., Labar, C., Menegatti, S., & Rao, B. M. (2021). Screening of yeast display libraries of enzymatically treated peptides to discover macrocyclic peptide ligands. *International Journal of Molecular Sciences, 22*(4). https://doi.org/10.3390/ijms22041634

46. Bacon, K., Bowen, J., Reese, H., Rao, B. M., & Menegatti, S. (2020). Use of target-displaying magnetized yeast in screening mRNA-display peptide libraries to identify ligands. *ACS Combinatorial Science, 22*(12), 738–744. https://doi.org/10.1021/acscombsci.0c00171

47. Reese, H. R., Xiao, X., Shanahan, C. C., Chu, W., Van Den Driessche, G. A., Fourches, D., Carbonell, R. G., Hall, C. K., & Menegatti, S. (2020). Novel peptide ligands for antibody purification provide superior clearance of host cell protein impurities. *Journal of Chromatography A, 1625*, 461237. https://doi.org/10.1016/j.chroma.2020.461237

48. Day, K., Schneible, J. D., Young, A. T., Pozdin, V. A., Van Den Driessche, G., Gaffney, L. A., Prodromou, R., Freytes, D. O., Fourches, D., Daniele, M., & Menegatti, S. (2020). Photoinduced reconfiguration to control the protein-binding affinity of azobenzene-cyclized peptides. *Journal of Materials Chemistry B, 8*(33), 7413–7427. https://doi.org/10.1039/D0TB01189D

49. Saberi-Bosari, S., Omary, M., Lavoie, A., Prodromou, R., Day, K., Menegatti, S., & San-Miguel, A. (2019). Affordable microfluidic bead-sorting platform for automated selection of porous particles functionalized with bioactive compounds. *Scientific Reports, 9*(1), 7210–7221. https://doi.org/10.1038/s41598-019-42869-5

50. Guangping, G., Vandenberghe Luk, H., Alvira Mauricio, R., You, L., Roberto, C., Xiangyang, Z., & Wilson James, M. (2004). Clades of adeno-associated viruses are widely disseminated in human tissues. *Journal of Virology, 78*(12), 6381–6388. https://doi.org/10.1128/JVI.78.12.6381-6388.2004

51. Mietzsch, M., Jose, A., Chipman, P., Bhattacharya, N., Daneshparvar, N., McKenna, R., & Agbandje-McKenna, M. (2021). Completion of the AAV structural atlas: Serotype Capsid structures reveals clade-specific features, *Viruses, 13*(1). https://doi.org/10.3390/v13010101

52. Wang, D., Zhong, L., Nahid, M. A., & Gao, G. (2014). The potential of adeno-associated viral vectors for gene delivery to muscle tissue. *Expert Opinion on Drug Delivery, 11*(3), 345–364. https://doi.org/10.1517/17425247.2014.871258

53. Hocquemiller, M., Giersch, L., Audrain, M., Parker, S., & Cartier, N. (2016). Adeno-associated virus-based gene therapy for CNS diseases. *Human Gene Therapy, 27*(7), 478–496. https://doi.org/10.1089/hum.2016.087

54. Blessing, D., Vachey, G., Pythoud, C., Rey, M., Padrun, V., Wurm, F. M., Schneider, B. L., & Déglon, N. (2019). Scalable production of AAV vec-

tors in orbitally shaken HEK293 cells. *Molecular Therapy – Methods & Clinical Development*, *13*, 14–26. https://doi.org/10.1016/j.omtm.2018.11.004

55. Nass, S. A., Mattingly, M. A., Woodcock, D. A., Burnham, B. L., Ardinger, J. A., Osmond, S. E., Frederick, A. M., Scaria, A., Cheng, S. H., & O'Riordan, C. R (2018). Universal method for the purification of recombinant AAV vectors of differing serotypes. *Molecular Therapy – Methods & Clinical Development*, *9*, 33–46. https://doi.org/10.1016/j.omtm.2017.12.004

56. Fan, J., Barbieri, E., Shastry, S., Menegatti, S., Boi, C., & Carbonell, R. G. (2022). Purification of adeno-associated virus (AAV) serotype 2 from *Spodoptera frugiperda* (Sf9) lysate by chromatographic nonwoven membranes. *Membranes*, *12*(10), https://doi.org/10.3390/membranes12100944

57. Overton, L., Boi, C., Shastry, S., Smith-Moore, C., Balchunas, J., Sambandan, D., & Gilleskie, G. (2023). Development and delivery of a hands-on short course in adeno-associated virus manufacturing to support growing workforce needs in gene therapy. *Human Gene Therapy*, https://doi.org/10.1089/hum.2022.235

58. Smith, R. H., Levy, J. R., & Kotin, R. M. (2009). A simplified baculovirus-AAV expression vector system coupled with one-step affinity purification yields high-titer rAAV stocks from insect cells. *Molecular Therapy*, *17*(11), 1888–1896. https://doi.org/10.1038/mt.2009.128

59. Glaser, V. (2013). Reducing the cost of peptide synthesis. *Genetic Engineering & Biotechnology News*, *33*(13), 32–34. https://doi.org/10.1089/gen.33.13.18

60. Bray, B. L. (2003). Large-scale manufacture of peptide therapeutics by chemical synthesis. *Nature Reviews Drug Discovery*, *2*(7), 587–593. https://doi.org/10.1038/nrd1133

61. Joshi, P. R. H., Bernier, A., Moço, P. D., Schrag, J., Chahal, P. S., & Kamen, A. (2021). Development of a scalable and robust AEX method for enriched rAAV preparations in genome-containing VCs of serotypes 5, 6, 8, and 9. *Molecular Therapy – Methods & Clinical Development*, *21*, 341–356. https://doi.org/10.1016/j.omtm.2021.03.016

62. Wang, Q., Lock, M., Prongay, A. J., Alvira, M. R., Petkov, B., & Wilson, J. M. (2015). Identification of an adeno-associated virus binding epitope for AVB sepharose affinity resin. *Molecular Therapy – Methods & Clinical Development*, *2*, 15040. https://doi.org/10.1038/mtm.2015.40

63. Dickerson, R., Argento, C., Pieracci, J., & Bakhshayeshi, M. (2021). Separating empty and full recombinant adeno-associated virus particles using isocratic anion exchange chromatography. *Biotechnology Journal*, *16*(1), 2000015. https://doi.org/10.1002/biot.202000015

64. Qu, G., Bahr-Davidson, J., Prado, J., Tai, A., Cataniag, F., McDonnell, J., Zhou, J., Hauck, B., Luna, J., Sommer, J. M., Smith, P., Zhou, S., Colosi, P., High, K. A., Pierce, G. F., & Wright, J. F. (2007). Separation of adeno-associated virus type 2 empty particles from genome containing vectors by anion-exchange column chromatography. *Journal of Virological Methods*, *140*(1), 183–192. https://doi.org/10.1016/j.jviromet.2006.11.019

65. Arunkumar, A., & Singh, N. (2021). Ultrafiltration behavior of recombinant adeno associated viral vectors used in gene therapy. *Journal of Membrane Science*, *620*, 118812. https://doi.org/10.1016/j.memsci.2020.118812

SUPPORTING INFORMATION

Additional supporting information can be found online in the Supporting Information section at the end of this article.